Title
Optical Absorption-Based In Situ Characterization of Halide Perovskites

Journal
Advanced Energy Materials, 10(26)

ISSN
1614-6832

Authors
Babbe, Finn
Sutter-Fella, Carolin M

Publication Date
2020-07-01

DOI
10.1002/aenm.201903587

Peer reviewed

aenm.201901879:

Special Issue “Halide Perovskites - Optoelectronic and Structural Characterization Methods”

Optical Absorption-Based *In Situ* Characterization of Halide Perovskites

*Finn Babbe[1,2] and Carolin M. Sutter-Fella[1]**

Dr. F. Babbe

[1] Chemical Sciences Division, Lawrence Berkeley National Laboratory, Berkeley, CA 94720, USA

[2] Joint Center for Artificial Photosynthesis, Lawrence Berkeley National Laboratory, Berkeley, CA 94720, USA

Dr. C. M. Sutter-Fella

[1] Chemical Sciences Division, Lawrence Berkeley National Laboratory, Berkeley, CA 94720, USA

E-mail: csutterfella@lbl.gov

Keywords: halide perovskites, *in situ* characterization, optical absorption, photoluminescence, UV-Vis

Halide perovskites have emerged as materials for high-performance optoelectronic devices. Often, progress made to date in terms of higher efficiency and stability is based on increasing material complexity that is, formation of multicomponent halide perovskites with multiple cations and anions. In this review article, the use of *in situ* optical methods, namely photoluminescence (PL) and UV-Vis, that provide access to the relevant time- and length-scales to ascertain chemistry-property relationships by monitoring evolving properties is discussed. Additionally, because halide perovskites are electron-ion conductors and prone to solid-state ion transport under various external stimuli application of these optical methods in the context of ionic movement, is described to reveal mechanistic insights. Finally, examples of using *in situ* PL and UV-Vis to study degradation and phase transitions are reviewed to demonstrate the wealth of information that can be obtained regarding many different aspects of ongoing research activities in the field of halide perovskites.

1. Introduction

Organic-inorganic metal halide perovskites received great research attention due to their outstanding optoelectronic properties,[1]–[5] bandgap tunability,[6][7] and ease of fabrication at low temperatures.[8] The family of metal halide perovskites crystallize in the ABX_3 structure where the most commonly used monovalent cations A are methylammonium (MA), $CH_3NH_3^+$, or formamidinium (FA), $CH(NH_2)_2^+$.[9]–[11] Mixtures thereof with some amount of alkali metals have shown promising performance and stability.[7][12][13] Typically, in the best performing devices the B site is occupied by Pb^{2+}. Alternatives like Sn^{2+} or Ge^{2+} have been tested but show lower device performance.[13] The X anions are typically halogens such as I^-, Br^-, Cl^-. Over the last decade rapid and impressive improvements have been made leading to solar power conversion efficiencies > 25%.[14] Recently also for single crystal solar cells high power conversion have been reported (21.9%) [15].

In this review, we discuss the use of non-destructive optical probes, in particular photoluminescence (PL) and UV-Vis, which are used by many laboratories for *ex situ* characterizations, but now with slight technical modifications to use them for *in situ* monitoring of evolving or changing optical properties. As an example, most of to dates' highest performing photovoltaic devices are based on chemical solution synthesis using spin coating technique to form polycrystalline thin films. The conversion processes during spin coating and annealing include wet film thinning, solvent evaporation causing supersaturation followed by nucleation and

growth, and finally, coarsening of the grains.[8] All these steps can influence final film properties including crystal structure, morphology, and electrical and optical properties. Thus, *in situ* monitoring of optical properties offers a powerful real time probe to capture dynamical processes that occur during spin coating and annealing. Given the fact that lead halide perovskites are not only electron but also ion conductors there is

substantial mass transport occurring in the sample depending on external stimuli such as light,

heat or electric fields.[16] *In situ* monitoring the optical response of the perovskite material with respect to the stimuli is instrumental in revealing mechanistic insights and designing strategies how to mitigate undesired ionic transport. Many recent *in situ* studies of halide perovskites have been employed to advance our understanding of dynamical processes related to halide perovskite formation, degradation, ionic movement and phase changes including diffraction measurements,[17]–[22] terahertz spectroscopy,[23]–[25] UV-Vis spectroscopy,[26]–[30] electron microscopy,[31] Raman,[32] and PL.[32]–[40]

Frequently, researchers use the terms “light soaking” or “continuous laser irradiation” when a sample is exposed to illumination (typically at fixed power and excitation wavelength) while recording PL or UV-Vis spectra over a certain time. While the term *in situ* is often used in relation with synthesis. The common concept however, is a process or sample under illumination with consecutive recording of optical spectra (PL, reflection, or transmission).

We begin this review by discussing challenges related to light being the experimental probe and best practices to limit probe-related effects and damage. Subsequently following are discussions on how *in situ* PL and UV-Vis can provide insights into nucleation, growth, thus providing process control, ion exchange reactions, degradation and phase transitions. This will be demonstrated not only on polycrystalline thin films but also on nanocrystals. In each section we will discuss a few research examples to illustrate application of *in situ* PL and UV- Vis. Finally, we identify future opportunities based on the simultaneous *in situ* recording of optical and

electrical properties for example, to provide a holistic picture revealing dynamics at different time and lengths scales including mechanistic insights under operating conditions.

2. Characterizing Halide Perovskites by Light Excitation

It is well known that halide perovskites are sensitive to several conditions including moisture, elevated temperatures, irradiation, oxygen, and electric bias.[32][35][36][41]–[48] Here we want to list how the optical probe (monochromatic and white light) may induce (reversible and irreversible) changes in metal halide perovskites. It will become obvious that there can be an interplay between light excitation, ion migration, and material degradation. Please note that this is not intended to be an exhaustive discussion including detailed understanding of why the described mechanisms happen. We rather want to sensitize the reader to probe-related effects and provide some best practices and recommendations for experimentalists.

The photophysical processes occurring in metal halide perovskites after light excitation at room temperature are schematically illustrated in Figure 1a. After excitation predominantly free charge carriers are generated, but likely also Wannier-Mott excitions.[1] The latter however will dissociate within picoseconds due to the low binding energy.[49] After thermalization to the band edges charge carriers are mobile giving rise to drift and diffusion. In the presence of trap states this leads to trapping, de-trapping as well radiative and non-radiative recombination of charge carriers within the bulk and at grain boundaries.[50] The combination of high charge carrier mobility and potentially high amounts of trap states can lead to trap filling which can drastically change carrier lifetimes and consequently

recombination properties, thus PL response.[1][51]

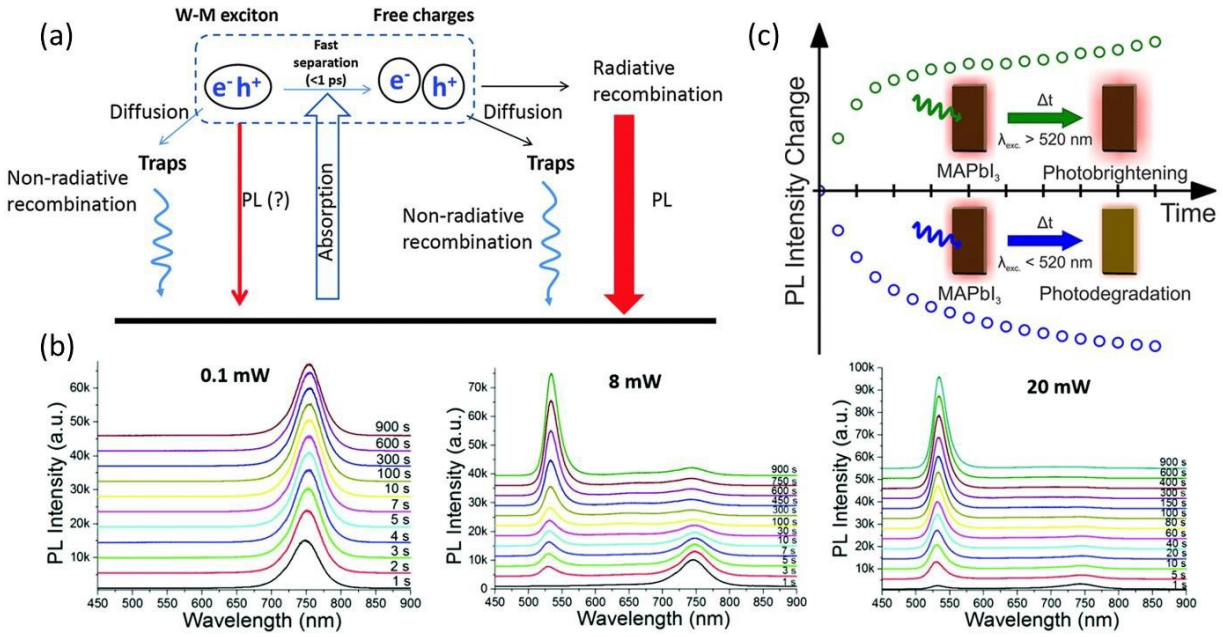

Figure 1: a) Schematic illustration of photophysical processes in halide perovskites after light absorption, starting with creation of free charges and Wannier-Mott excitons followed by de-excitation processes. Adapted with permission.[52] Copyright 2015, Royal Society of Chemistry. b) Power dependent change of PL spectra of mixed $MAPbI_1Br_2$ films under constant continuous wave laser illumination (407 nm) over 900 s. Reproduced with permission.[32] Copyright 2018, American Chemical Society. c) PL intensity change over time when illuminating a $MAPbI_3$ sample with excitation wavelength larger than 520 nm (photo-brightening) or smaller than 520 nm (photo-degradation). Reproduced with permission.[36] Copyright 2019, Royal Society of Chemistry.

Sample illumination can have several effects which are dependent not only on external factors such as laser excitation power, excitation wavelength, and atmosphere, but also on internal factors such as trap density and elemental composition.[32][35][36][47][53]–[61] Importantly, these effects can have mutual dependencies. The light dose for example can reduce the trap density (by an order of magnitude),[54] with the measurement environment being likely the cause for trap formation or passivation.[55][62] Photo-induced ion migration is another example of probe- related effects[53][54] that plays a critical role and leads to significant changes in optical properties caused by the laser illumination.[32]

Ruan et al.[32] investigated the influence of probe-related effects and showed that the kinetics of halide segregation severely depend on the laser power (Figure 1b). It should be considered that the usage of a focused laser beam often results in significantly higher intensities than experienced under solar equivalent illumination and these higher intensities can lead to

illumination induced degradation over time. Photostability was found to be composition dependent. In addition, sample degradation is highly laser wavelength dependent with shorter wavelength illumination causing more damage at a fixed power.[32][36] Quitsch et al.[36] found photo-brightening or -degradation for $MAPbI_3$ samples depending whether they are exposed to a laser light with wavelengths larger or smaller than 520 nm, respectively (Figure 1c). Besides the number of photons absorbed, the photon energy thus plays a critical role.[32] It is debated to which extend continuous illumination versus pulsed illumination influences halide segregation.[55][63]

Further, it is important to know that photochemical reactions in the presence of O_2 have been reported.[32][35][52][64][65] Since the proposed mechanism involves the formation of a superoxide O_2^- which can fill in iodide vacancies, not only the measurement environment but also the number of vacancies (i.e. defects) matter. As an example, a thousand-fold boost of initial PL yield as an effect of light curing with O_2 was measured. [52] In this context, the chemical composition of the perovskite sample also plays a role. For example $MAPbBr_3$ exhibits better photostability than $MAPbI_3$ in both, air and N_2.[32] Additionally, the PL intensity of perovskite films measured in vacuum can change over time under constant illumination.[35][55] Lastly, PL enhancement was not only reported with dependence on the atmosphere but also on crystal size.[52]

Another probe related degradation process could be caused by local heating due to high laser power densities. Using Raman measurements on single crystals, it was found, that the effects of light versus heat

degradation are different with decomposition under laser irradiation being much more severe than under elevated temperature.[32] Again, chemical composition influences thermal stability, where $MAPbBr_3$ exhibits higher thermal stability than $MAPbI_3$.[32] In another study, halide segregation was investigated at low temperatures to evaluate to which extend laser heating is involved in this phenomenon.[53] The authors excluded that laser heating is

responsible for the observed spectral changes under laser light.[53] As a final point, we want to briefly mention probe-induced sample modifications when multiple probes such as electron beam and laser illumination are used together or simultaneously.[64][66] Significant changes in PL have been observed due to scanning electron beam exposure including a dependence on sample morphology.[52][64]

Given these many effects which potentially overlap or have mutual dependencies, research results might show apparent discrepancies. One possible explanation could be the lack of reporting complete experimental conditions. Therefore, it is highly recommended that measurements are taken with great diligence. For each sample and each setup, the user needs to investigate effects of laser illumination for the excitation wavelength used in the respective study. Cross checks at different excitation powers under time dependent illumination are highly recommended. Depending on the goal of the study, it might make sense to find measurement conditions with least degradation and impact on the sample in order to ensure reliable and reproducible results. To avoid reaction with the atmosphere, film encapsulation with Polymethyl methacrylate (PMMA) is recommended. Finally, for the reporting of results, as many experimental details as possible need to be given including not only excitation wavelength and power, but ideally power density at the sample position. Further the measurement atmosphere and information related to the history of the sample (such as sample was kept in the dark for x amount of time under y atmosphere) should be given.

3. Photoluminescence

Photoluminescence (emission of light after photon excitation) is a versatile non-destructive optical phenomenon with many experimental variants. Given the high absorption coefficient of metal halide perovskites of > 10^5 cm^{-1} for wavelengths above the bandgap,[67] the absorption depth is less than 100 nm which is smaller than the typical film thicknesses of 300-500 nm used for photovoltaic devices.[8] A detailed overview about the general optical processes involved in semiconductors can be found in chapter 7 of reference[68] and in reference.[69] More general guidance on the detection and interpretation of PL spectra can be found in chapter 7 of reference [70] and in reference.[71]

Since the most basic PL measurement requires only a few components, namely, a monochromatic illumination source and a detector/spectrometer (Figure 2a), many laboratories use PL spectroscopy to characterize perovskite films and nanocrystals. Using more advanced setups, PL can be also combined with other measurement techniques like UV-Vis or performed during spin coating or annealing processes (Figure 2b).

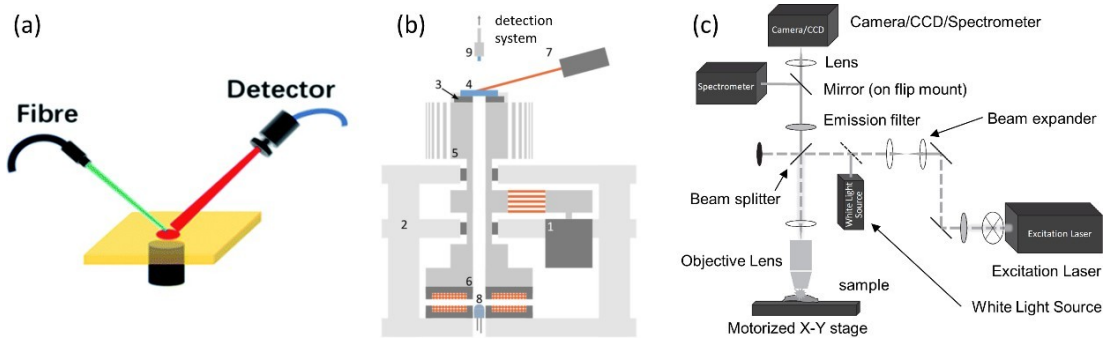

Figure 2: a) Schematic of the most basic PL setup consisting of a monochromatic light source, the sample and a detector. Reproduced with permission.[72] Copyright 2018, Royal Society of Chemistry. b) Schematic of a PL setup with integrated spin coater device (5), hot plate (3) and white light source (8) for transmission measurement for comprehensive in situ characterization. Designed and built by Buchhorn et al. Reproduced with permission.[73] Copyright 2018, Royal Society of Chemistry. c) Schematic of a micro PL

setup with additional imaging capabilities. Adapted with permission.[71] Copyright 2018, Cambridge University Press.

The simplest form of PL measurements is carried out in steady state condition using a continuous, pulsed or chopped illumination for charge carrier excitation. The light source

chosen for this is typically a laser source or a LED with a narrow emission spectrum. The generated luminescence is then guided to a spectrometer commonly using some kind of collection optics and an optical fiber. Within the spectrometer the light is spectrally resolved and guided to a detector. Detection is mostly done in one shot using Silicon or InGaAs-detector arrays but alternatively can also be done stepwise by scanning though the wavelengths and using a photomultiplier (or another detector). The measurement time for sufficient signal-to- noise ratios is strongly dependent on the excitation density, radiative efficiency of the probe as well as the setup geometry and specifications (especially numerical aperture, alignment and the diameter of the optical fiber). As a rough guideline, using a photon flux similar to the AM1.5 sun spectrum measurement time below 1 seconds are feasible depending on sample quality.

Spectrally resolved PL of perovskites at room temperature generally exhibit one broad peak corresponding to the band-to-band transition of the semiconductor. The energy of the peak maximum can in first approximation be interpreted as the bandgap of the sample.[70][74] The peak width is dependent on the temperature, internal strain, Urbach tailing, and Froehlich interaction between charge carriers and longitudinal optical (LO) phonons.[68][70][74][75] The Urbach energy can be derived by analyzing the low energy part of a PL spectrum (for example shown in reference [76]) which among other things is affected by shallow defects, disorder in the semiconductor and bandgap fluctuations. If a setup is calibrated correctly the absolute number of photons per second and

square centimeter can be derived allowing the determination of the external radiative efficiency (also named PL quantum yield (PLQY) or PL efficiency (PLE)). This quantity is on the order of a few percent for good quality absorber layers[50][77][78] and is directly linked to the quasi Fermi level splitting and the implied voltage of a solar cell.[79][80] On a side note it should be mentioned that the interpretation of PL spectra can be impeded by thin film interference effects,[81][82] insufficient background correction as well as drifting spectrometer calibrations.

Spatially resolved PL images can be obtained by either using a micro PL setup with a scanning probe station (Figure 2c), or by using a lens for widefield imaging in combination with a camera. Commonly CMOS or silicon cameras are used for the latter, enabling fast data acquisition and short measurement times. However, the PL signal is then integrated and the information about the energy distribution is lost. A hyper spectral image where each pixel represents a full spectrum can be achieved by either scanning across the sample and measuring a spectrum for each point (spatial scanning) or by various bandpass filters to measure different energy regimes after each other (spectral scanning). A third option is to use a grating in front the camera and to use the first order diffraction to gain information about the position and intensity as well as the second order diffraction to get spectral information.[83][84] Depending on the microscope type used (wide field, confocal, super resolution) and the post-processing applied, resolution from a few tens of micrometers to below the diffraction limit are possible.

3.1 Monitoring of Synthesis

The chemistry and synthetic details of halide perovskite materials not only play a crucial role for final device performance but also for stability, morphology, phase formation, as well as electrical and optical properties. The growth of crystalline perovskite films involves several complex processes for which no general theories have been established.[8] In this regard, steady state *in situ* PL measurements during synthesis of halide

perovskite thin films or nanocrystals present a valuable tool to shed light on synthesis mechanisms, nucleation and growth, and to establish precursor chemistry – property relationships. In this part, we will discuss a few synthesis examples were *in situ* PL was used to track perovskite thin film and nanocrystal formation. Figure 3 shows a selection of *in situ* PL measurements demonstrating the variety of processes that can be monitored and data extracted.

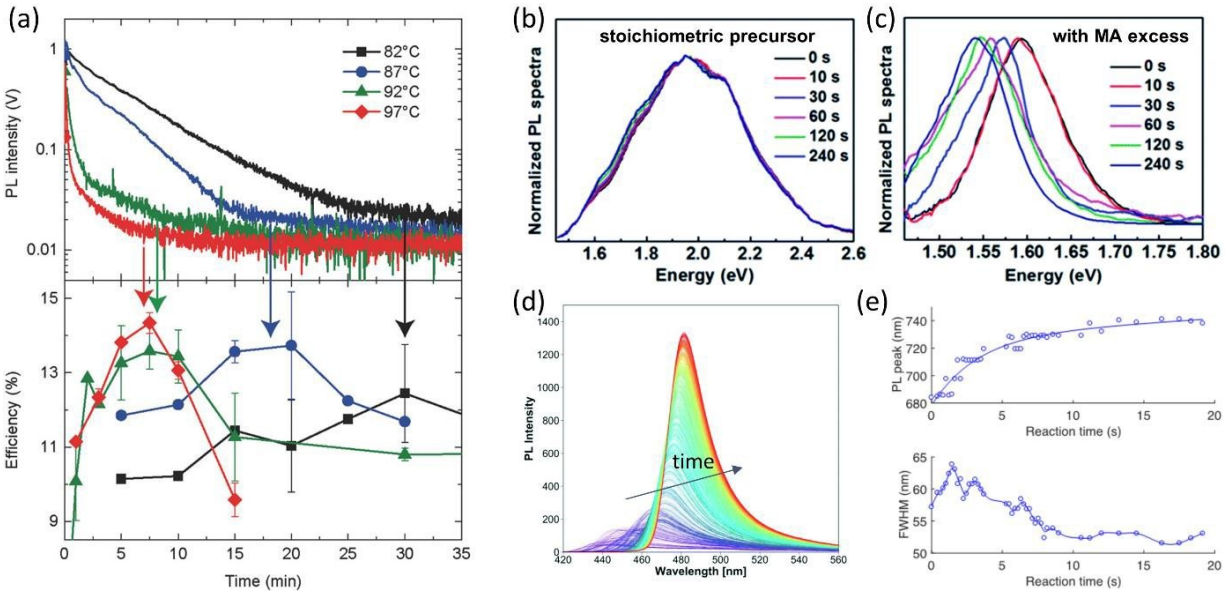

Figure 3: a) Evolution of the PL intensity depending on the annealing temperature and correlation to device efficiency for each temperature/time combination. Reproduced with permission.[33] Copyright 2016, Wiley-VCH.
b) Synthesis of $FA_{1-x}MA_xPbI_3$ films using a stoichiometric (left) versus c) over-stoichiometric MAI-rich (right) precursor. Adapted with permission.[72] Copyright 2018, Royal Society of Chemistry. d) Shift of PL spectra after benzoyl bromide injection initiating $CsPbBr_3$ nucleation and growth. Reproduced with permission.[39] Copyright 2019, Royal Society of Chemistry. e) Evolution of PL peak position and corresponding FWHM during nanocrystal growth. Reproduced with permission.[85] Copyright 2018, American Chemical Society.

Optimization of thermal annealing (duration and temperature) is a crucial step during synthesis and precursor conversion to form halide perovskites.[8][22][33][86][87] Franeker et al.[33] used *in situ* PL to study formation of $MAPbI_3$ layers deposited by a hot casting method in air and correlated observations to solar cell efficiency. In particular the PL quenching, that is charge carrier recombination, was investigated on glass/PEDOT:PSS/$MAPbI_3$ architectures during annealing of the perovskite film. It was found that the PL intensity decay showed a very fast, temperature dependent, exponential component at the beginning followed by a slower decay behavior (Figure 3a). The authors suggested two different mechanisms to explain this observation: changes in chemical

composition and in crystal habit and size. The highest annealing temperature studied (97 °C) for about 7 min resulted in the highest power conversion efficiencies.[33]

In situ PL is also helpful in evaluating new synthesis pathways for example using non- stoichiometric instead of stoichiometric precursors with mixed organic cations. Enabled by *in situ* PL, Xie et al.[72] found that if a stoichiometric precursor is used to form (FA,MA)PbI_3 an amorphous precursor phase appeared with a PL peak at 1.97 eV and a broad full width at half maximum (FWHM) (Figure 3b). This peak is linked to the formation of the unfavorable δ-phase as shown by XRD which can only be converted to the desired α-phase by annealing. Conversely, the reaction with excess MAI (over-stoichiometric precursor) resulted in direct formation of $MAPbI_3$ (PL peak at 1.59 eV) followed by a gradual peak shift to lower energy (Figure 3c). The smaller molecular mass size of the MA likely facilitates the direct formation of the α-phase due to the easier penetration of the PbI_6 framework. The shift towards lower energies originates from the substitution of MA by FA. From those observations, it was concluded that the ion exchange when using excess MAI starts early on at the liquid-to-solid state transformation. In this example, PL is particularly powerful to shed light on the early stages of crystallization where often amorphous materials form first and thus XRD has limitations.

Wagner et al.[88] monitored the 2-step reaction process where first PbI_2 is formed to react with MAI in the second step by *in situ* PL and external quantum efficiency (EQE). The authors distinguished 3 phases. Initially, the PL intensity increases and red-shifts which is attributed to crystal growth. In the second phase the PL intensity decreases caused by quenching boundary effects and finally PL stabilizes in the third phase. Interestingly, high PL intensity did not correlate with the simultaneously measured

photocurrent. Only after the PL intensity stabilized, the photocurrent increased which is explained by improved surface alignment between the perovskite and the contact layers.

Protesescu et al.[89] used *in situ* PL to track the fast nucleation and growth of $CsPbX_3$ (X = I, Br, Cl) nanocrystals and conclude that the majority of the growth is completed after 1-3

seconds, the faster the heavier the halides. The typical PL features observed during nanocrystal

synthesis are a broad peak at high energy stemming from surfactants. As soon as formation is triggered (e.g. by hot injection or halide precursor injection) red shifting of the PL maximum and peak narrowing is observed until PL emission wavelength is constant indicating nucleation and growth until growth is terminated (Figure 3d).[39][90] It was concluded that the size of the nanocrystals cannot be controlled by the growth time but is controllable with the reaction temperature.[39][89] In these studies nucleation kinetics were not quantified, nor attempted to interpret via classical nucleation theory but the results demonstrate that *in situ* PL could be used to extract detailed kinetics with respect to synthesis condition such as temperature or chemical composition. In a separate study in the domain of nanocrystal synthesis, *in situ* PL has been used successfully for parametric screening of quinary $Cs_xFA_{1-x}Pb(Br_{1-y}I_y)_3$ compositions with the goal to optically engineer and fine tune emission between 700-800 nm.[85] This example demonstrates how *in situ* PL can be implemented in high throughput experimentation to enable compositional (PL peak position) and quality control (PL FWHM and PL quantum yield) during synthesis (Figure 3e)[85][91] as well as for the screening of synthetic conditions such as temperature and ligand ratio.[39]

Next, *in situ* PL measurements can be very powerful in monitoring chemical composition tuning

i.e. ion exchange reactions at the cation or anion site. Cation exchange such as Cu, Cd, In, and Zn is well studied in nanocrystals and often results in better material properties compared to the initial material.[92] This strategy can enable compositions which are difficult to synthesize directly

from the precursor. Pellet et al.[93] used PL emission to track halide substitution in the crystal lattice of $MAPbX_3$ (X = Cl, Br, I) by other halides via dipping of the perovskite film in MAX dissolved in anhydrous 2-propanol (Figure 4). It was found that the anion in the dipping solution dictates final halide composition with the chemical potential difference as the driving force. The PL and diffraction peak positions were used to extract compositional information

i.e. the I:Br ratio. Conversion from $MAPbBr_3$ (characterized by PL emission at 535 nm or

2.32 eV) to $MAPbI_3$ (characterized by PL emission at 760 nm or 1.63 eV) shows a sharp red

shift in the beginning (Figure 4a) which would correspond to a much higher iodide content than indicated by XRD measurements. Consequently, the PL peak position was hypothesized to be caused by local iodide-rich domains which funnel carriers where they eventually recombine. Full substitution of Br by I is not achieved even after 1 hour of reaction. Interestingly, the reaction in the other direction, from $MAPbI_3$ to $MAPbBr_3$ advances faster due to the favorable thermodynamics, crystal lattice shrinkage and higher surface area (Figure 4b). The blue-shift in PL correlates with XRD. However, no PL signal was observed between 535 – 609 nm which was explained by a PL inactive composition window given that XRD reflections continuously shift. Full anion exchange was confirmed by XRD after 5 minutes while PL indicated much faster completion. This discrepancy was attributed to local laser heating facilitating a faster anion exchange. In nanocrystal synthesis, Nedelcu et al.[94] found very fast anion exchange (several seconds) in the $CsPbX_3$ (X = Cl, Br, I) system with high PL quantum yield throughout the exchange reaction. Similarly, fast cation exchange has been reported in the $(MA,FA)PbI_3$ system.[95] Exposure to the other cation resulted in PL peak broadening which was attributed to structural disorder or a strained perovskite phase.

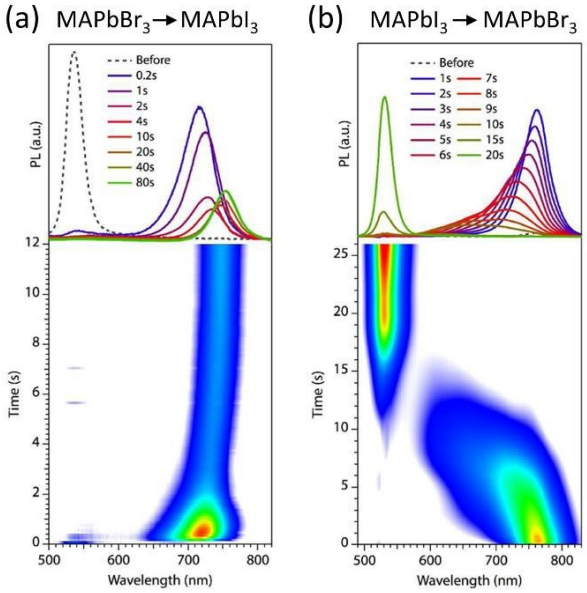

Figure 4: Time evolution of ion exchange reaction revealed by in situ PL. a) conversion from $MAPbBr_3$ to $MAPbI_3$, and b) from $MAPbI_3$ to $MAPbBr_3$. Upper part: individual spectra, lower part: corresponding contour plots. Reproduced with permission.[93] Copyright 2015, American Chemical Society.

Overall *in situ* PL measurements are a valuable tool to investigate and control early nucleation and crystallization processes as well as ion exchange reactions. As materials likely form amorphous phases initially, PL can provide more information than diffraction measurements. Use of PL to monitor compositional changes can be instrumental given the correlation between bandgap and for example halide composition. However, it is a double-edged sword because light can induce local halide segregation resulting in locally different composition than in the bulk.

3.2 Light Soaking Effects, Ion Migration and Sample Degradation

In situ PL monitoring is not only a powerful method to investigate synthesis with the quest to unveil mechanistic insights, understand the role of precursor chemicals, or study growth kinetics, but also capable of probing photophysical processes. Here we focus on light induced effects and how to understand them. In this regard, researchers often use the terms light soaking, continuous laser irradiation or continuous optical excitation instead of *in situ* PL, when a sample is exposed to illumination (continuous or pulsed excitation) at fixed power and excitation wavelength while recording PL spectra over a certain time.

One of the most effective strategies to tune the bandgap of metal halide perovskites over a large portion of the visible spectrum is via halide substitution.[6][13][96] Although substitution of iodide with bromide increases the bandgap, a corresponding increase in open-circuit voltage (V_{OC}) was not found.[6] The reason for the so called V_{OC} deficit was explained by Hoke et al.[53] who found that mixed $MAPb(I_{1-x}Br_x)_3$ exhibit light-induced,

reversible, transformations into iodide- and bromide-rich domains. In fact, continuous monitoring via PL over 45 s in 5 s increments revealed that an additional peak forms at lower energy which increases in intensity over time (Figure 5a). This finding was the first indication that halides are highly mobile in $MAPb(I,Br)_3$. It triggered a lot of research interest and *in situ* PL was and still is a highly useful tool in the attempt to understand halide movement.[55][76][97]–[99] Following the evolution of the PL signal

was instrumental in concluding that light-induced halide segregation is triggered by electric fields as a consequence of trapped charge carriers and may be enhanced by carrier funneling into the lower energy iodide-rich domains.[55] Ruan et al.[32] found that exposure to high illumination power leads to decomposition of I-rich domains and consequently recombination occurs via Br-rich domains (emission ~530 nm).

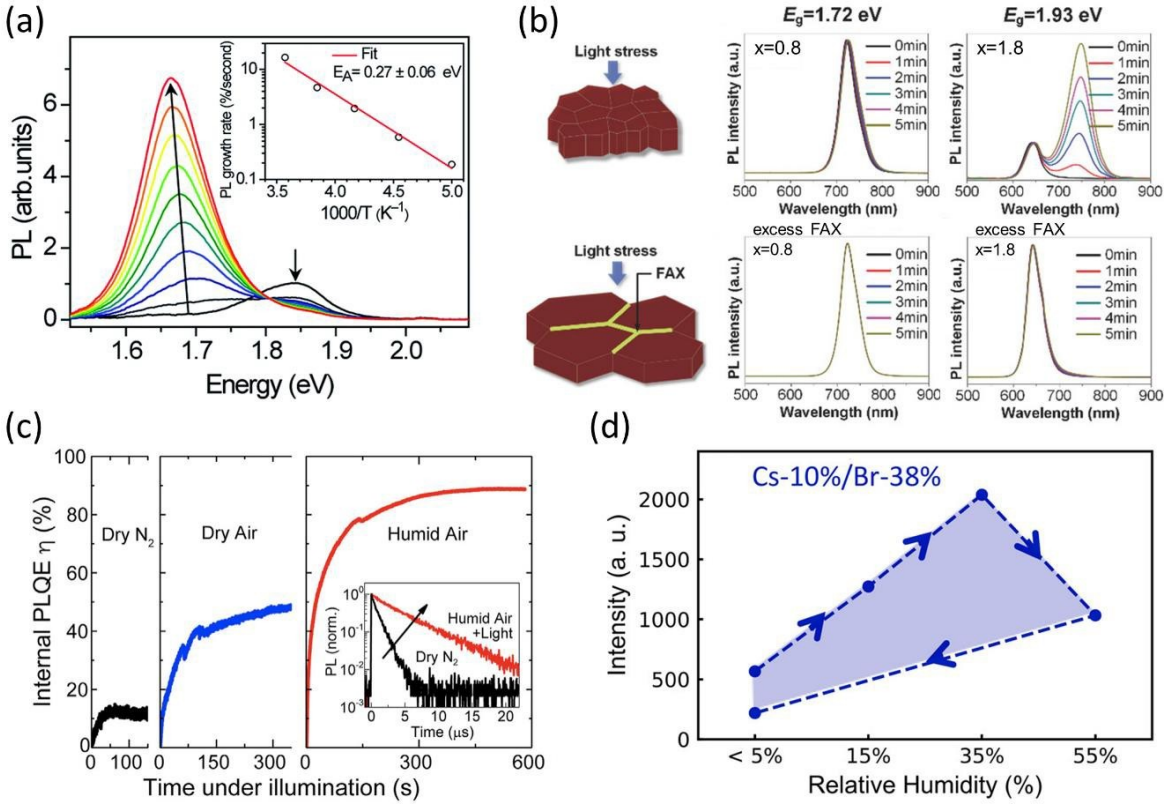

Figure 5: a) Evolution of PL spectra continuously taken on a $MAPb(I_{0.6}Br_{0.4})_3$ sample. Reproduced with permission.[53] Copyright 2015, Royal Society of Chemistry. b) PL spectra of $FA_{0.17}Cs_{0.83}PbI_{3-x}Br_x$ films with increasing Br content (x = 0.8 and 1.8) and precursor solution engineering ($Pb(SCN)_2$ with excess FAX (X = I, Br) in the bottom case). Reproduced with permission.[100] Copyright 2018, Wiley-VCH. c) PL intensity change over time under different atmospheric conditions. Reproduced with permission.[101] Copyright 2017, Elsevier B.V. d) Composition dependent PL hysteresis under different relative humidity levels. Reproduced with permission.[102] Copyright 2018, American Chemical Society.

In reverse, *in situ* PL can provide mechanistic insights into photostability and how to improve it for example by compositional tuning or passivation strategies. In this regard, Barker et al. demonstrated that ion segregation

is facilitated by halide defects.[99] Moreover, via continuous PL monitoring they found that halide segregation can be suppressed by controlling the light distribution or the defect density in the film.[99] Zhou et al.[100] compared PL intensity change

over time in wide-bandgap $Cs_{0.17}FA_{0.83}PbI_{3-x}Br_x$ (x = 0.8, 1.2, 1.5, and 1.8) perovskites and found better stability under illumination when synthesized with FAX (X = I, Br) excess (Figure 5b). A synergistic effect between larger grain size, reduced number of impurities, and passivated grain boundaries was suggested to explain superior photostability.[100] In another example, improved photostability in $CsPbI_2Br$ was found using a functionalized cathode interlayer and was explained by passivated electronic surface trap states.[103] Also the suppression of ion migration using oxygen to passivate halide vacancies has been shown.[52][104] There are multiple reports on photochemical reactions or chemisorption where the perovskite film starts to react at the surface with the surrounding atmosphere under light. This has been shown by *in situ* PL measurements where an intensity change over time was observed if perovskite samples were measured in air, moisture, N_2, O_2, or vacuum (Figure 5c).[32][35][52][55][65][101] These processes are suggested to be rate limited depending on (i) the light absorption depth which causes photoinduced iodide migrations and consequently a gradient in iodide vacancies with the largest density at the surface, and (ii) diffusion of the atmospheric atomic species i.e. O_2.[35] An in depth photophysical understanding of underlying processes can be enabled via PL measurements and we describe a few reports here although plenty reports are devoted to this phenomenon. Note that some of the results are contradicting and there is currently no clear consensus on the impact of light in combination with a specific environment.[35]

Early on, Galisteo-López et al. and others reported that O_2 in the

atmosphere is crucial for substantial PL enhancement in $MAPbI_3$.[52][65] Further, for $MAPbI_3$, light and atmospheric exposure was found to impact PL intensity negatively in N_2/vacuum but leads to an enhancement in O_2 and/or humidity.[35] Backed up by density functional theory calculations findings were explained by little change in the surface band structure upon N_2 or H_2O adsorption but a large reduction in trap states when O_2 is adsorbed.[35] Further, N_2 has little

effect on PL because it is unable to undergo a redox activity or a surface conversion reaction as

O_2 and H_2O, respectively, can do.[35] O_2 is photochemically reduced to O_2^- which is similar in size as the iodide ion and thus, effectively occupies iodide vacancies.[101] In contrast, light and O_2 induced degradation of mixed halide perovskites $MAPbI_xBr_{3-x}$ via deprotonation reaction of the MA-cation was suggested recently.[32] In moisture, removal of surface trap states upon surface conversion into a hydrate phase was found.[35] The nature of the specific grain that is dark/bright grains also matters and is discussed later. The impact of the environmental conditions in $Cs_xFA_{1-x}Pb(I_yBr_{1-y})_3$ perovskites was studied by Howard et al. [102] They found humidity-induced PL intensity hysteresis curves (Figure 5d) [102] and composition dependent (Cs/Br ratio) PL enhancement under different relative humidity levels.[102] In a different study on $FAPbI_3$ it was stated that the PL enhancement effect depends on the interplay between moisture-assisted light-healing and moisture-assisted degradation and correlates with the humidity level and laser power.[105] Song et al., used *in situ* PL to elucidate the degradation mechanisms in high humidity and divided it in four stages ($MAPbI_3$ case): humidity-assisted surface passivation, followed by n-type doping, formation of the monohydrated perovskite interface and finally, conversion to the hydrate phase.[106] As a last example and to showcase how phenomena are interconnected, Knight et al. reported that the halide segregation dynamics strongly depend on the atmospheric environment.[55] Their results suggest that light-induced halide segregation is triggered by electric fields which arise from trapped charge carriers.[55]

3.3 Lateral Variations and Heterogeneities

More insights about afore mentioned phenomena such as phase segregation under illumination and other stressors can be gained when investigated by spatially resolved PL. For instance Zhao et al.[37] studied the usage of perovskite seed crystals in a PbI_2 precursor layer. This approach has the advantage that cesium (incorporated in the seed crystals) can be homogenously incorporated into the films, strongly enhancing the stability of the perovskite absorber, and that the crystals act as sources for crystal growth overcoming energetic barriers employed by Gibbs

free energy. In this study laterally resolved PL was used to confirm the uniformity of seed crystals in the seed layer and additionally to investigate film growth during synthesis *in situ*. In the initial PL image of the seeding layer (Figure 6a) the bright spots correspond to seed crystals. Those crystals facilitate fast and homogenous layer growth within seconds (Figure 6b-c). The growth rate is much faster at seed crystals than for random nucleation (red circle in Figure 6b) and was estimated with this method to be about 1 µm s^{-1}. After a total of 13 s the film is completely formed (Figure 6c) showing the rapid growth of perovskites.

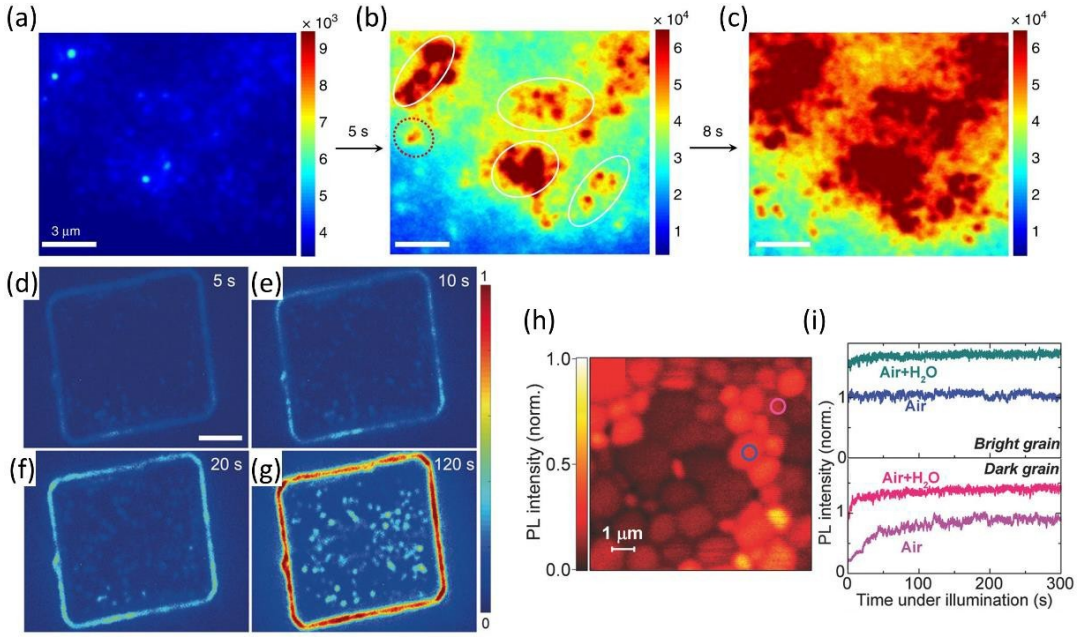

Figure 6: a-c) PL imaging during growth of a mixed hybrid perovskite from a seed crystal containing PbI_2 layer. White circles indicate spots with seed crystals and the red circle growth without. Reproduced with permission. *[37]* Copyright 2018, Nature Publishing Group. d-g) PL maps of a $MAPb(Br,I)_3$ crystal under constant illumination measured over time. Investigated is only luminescence in the wavelength region from 660 to 700 nm, corresponding to the emission from an iodine-rich phase. The scale bar represents 5 µm. Reproduced with permission.*[60]* Copyright 2019, Wiley-VCH. h) Integrated PL map of a $MAPbI_3$ perovskite film with distinguishable dark and bright grains. i) Light soaking behavior of a dark and bright grain over time under dry and humid conditions. Reproduced with permission. *[35]* Copyright 2018, Wiley-VCH.

Mao et al.[60] applied hyperspectral imaging to investigate the light soaking

and phase segregation processes in $MAPb(Br,I)_3$ single crystals which has been discussed previously for thin films. Initially, the crystals show luminescence around 550 nm corresponding to a mixed phase with a high bromide content. Under continuous illumination the shape of the spectrum

changes and a second peak around 700 nm appears, corresponding to PL from an iodide-rich

phase. Investigating the lateral distribution of PL from this iodide-rich phase (660 nm to 700 nm) an increasing signal at the edge of the crystal is observed under continuous blue illumination (Figure 6d-g). Applying the same technique to thin films yields similar results as shown by Tang et al.[107] They found that with ongoing illumination the PL spectrum of bulk grains does not exhibit any peak shift or strong luminescence quenching. However, the luminescence emitted from the grain boundaries showed the known appearance of a secondary peak over time at lower energies commonly attributed to an iodide-rich phase. Both studies thus directly show phase segregation of iodide mainly towards the grain boundaries. On a larger scale of several tens of micrometer Zhong et al.[108] showed the light driven formation of well luminescent and non-luminescent spots. In the latter case a migration of the mobile iodide ions towards the un-illuminated back site driven by the optical field induced by the illumination is proposed.

Also for the $MAPbI_3$ ternary strong ion migration has been shown[109] and lateral PL studies revealed strong differences in between grains[35][110][111] as well as on larger scales.[111]–[113] Pioneering work by deQuilettes et al. [110] showed by combining SEM and confocal PL that even for high quality materials the PL signal between grains strongly varies and that grain boundaries are not as benign as assumed. Time resolved PL measurements indicate faster carrier recombination and higher trap densities in dark grains, possibly linked facet orientation.[114] Brenes et al. [35] picked up this work and in detailed looked how the properties of dark and bright grains change under illumination in dry or humid atmospheres

(Figure 6e-f). If those film are exposed to N_2 the PL of both, light and dark grains, initially drops slightly. Measured in humidified N_2 bright grains slightly improve whereas dark grains nearly show doubled PL emission intensity, having similar yields to bright grains in the end. The same experiment carried out with compressed air, meaning that O_2 is available, shows that PL emission of bright grains is stable in air whereas for dark grains again a strong improvement is observed. If furthermore humidity is added both dark and bright grains show further PL enhancement

(Figure 6f). Looking at the local lifetimes an improvement in both atmospheres after the introduction of moisture is observed. Those results show that a reduction of non-radiative recombination especially in dark grains with a higher defect density can be reached by exposure to humidity and O_2 under illumination. In the dark no or much slower reactions are observed, showing the key role of illumination for the improvements in optical properties. Theoretical calculations explain this by the binding of O_2 to iodide vacancies. In case of humidity the formation of a passivating film on the surface is postulated. Those findings for the local behavior under various conditions could only be found by *in situ* PL measurements and contributed strongly to the understanding of light soaking and degradation mechanisms.

Spatially resolved PL measurements combined with time resolved PL measurements are powerful tools to study local recombination kinetics and local optical properties. With hyperspectral imaging especially phase segregation can be studied in detail, directly showing the ion migration towards grain boundaries but it is also useful to reveal growth dynamics and determine growth rates.

3.4 Monitoring Phase TransitionsInduced by Temperature and Pressure

This last section about PL focusses on the investigation of phase transitions induced by temperature and pressure. The investigation of phonon coupling will be briefly mentioned but the classical use of low temperature PL for defect spectroscopy will not be discussed here, as it is

not within the scope of this review.

Most halide perovskites are polymorphic materials exhibiting temperature dependent phase transitions. For example, the phase transition from orthorhombic to tetragonal structure in $MAPbI_3$ happens between 130 and 150 K and can be monitored by PL due to distinct bandgaps. A good example for this type of measurements has been published by Wright et al.[115] who

investigated the (MA,FA)Pb(I,Br)$_3$ composition (Figure 7a-d). The phase transition can be best seen looking at the peak position which for decreasing temperatures first shows a red shift. For all compositions studied this peak shift changes into a blue shift around 150 - 170 K indicating the phase transition to an orthorhombic structure. Depending on the composition, the formation of the low temperature phase can also be seen by the formation of a new emission peak as observed for MAPbI$_3$ (Figure 7b) and shown for MAPbCl$_3$ in other studies.[116][117]

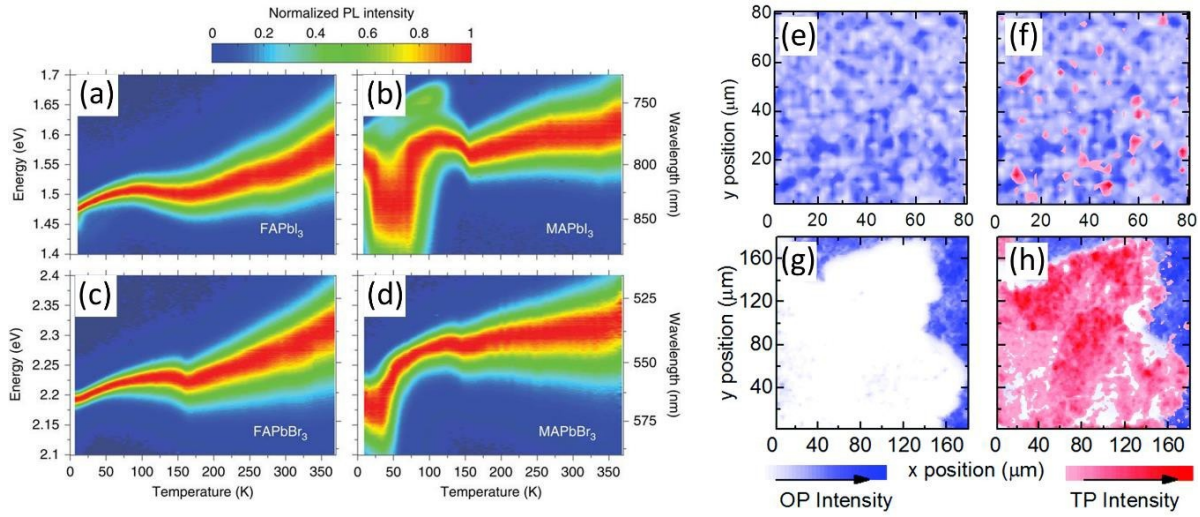

Figure 7: a-d) Normalized PL heat maps of several perovskite composition plotted over temperature. Reproduced with permission [115]. Copyright 2016, Nature Publishing Group. (e-h) False color image of a MAPbI$_3$ e,f) and a FAPbI$_3$ g,h) sample with blue representing luminescence from the orthorhombic phase (OP) and red from the tetragonal phase (TP). Reproduced with permission. [38] Copyright 2017, Royal Society of Chemistry.

From the same measurements conclusions about the phonon interaction can be derived by plotting the linewidth over temperature and fitting a model. The model describes the scattering of charge carrier and phonons as outlined in several publication.[115][118]–[121] This model accounts for a temperature independent broadening from imperfections, a broadening from acoustical phonons, a broadening from optical phonons and from

scattering of ionized impurities. From the fitting it can be derived that the Fröhlich interaction between charge carriers and optical phonons is the main contribution to the observed linewidth broadening in the investigated hybrid perovskites. Similar results have also been shown for $FAPbBr_3$ [119] and $FAPbI_3$ nanocrystals.[118] The existence of those longitudinal optical phonons was directly

shown by Fu et al.[120] They investigated $FAPbI_3$ nanocrystals at low temperature and observed three distinct phonon replicas of an excitonic transition.

In order to investigate crystal phase transitions laterally Galkowski et al.[38] combined temperature dependent measurements and hyperspectral PL imaging. They studied several compositions in the $(MA,FA)Pb(I,Br)_3$ material system. All investigated compositions exhibit the low temperature phase transition from tetragonal to orthorhombic, however not all crystallites change into the orthorhombic structure. Especially for $MAPbI_3$ samples about 20 % of the probed region shows PL footprints of the tetragonal phase even at 4 K (Figure 7e-f). Doping with aluminum significantly reduces incomplete phase transformation and the authors claim this is the origin for a 2% higher power conversion efficiency. The study also showed that the $FAPbBr_3$ system, which at room temperature shows a similar distribution of luminescence spots compared to $MAPbI_3$ and $FAPbI_3$, behaves quite different at low temperatures. At low temperature, macroscopic regions of more than 100 micrometer form which consists of tetragonal or orthorhombic phase (Figure 7g-h). The formation of such large domains is speculated to be related to the small difference in free energy between the phases for this composition likely allowing the phase transition to propagate more easily.

PL is also a powerful tool to study phase transitions induced by pressure. Wang et al.[122] showed

with *in situ* PL and UV-Vis measurements that the bandgap transition of $MAPbI_3$ at atmospheric pressure at room temperature is indeed indirect

and only with increasing pressure a direct bandgap forms which is about 60 meV larger than the indirect transition. The low energetic difference between the two bandgaps allows a high absorption coefficient as well as a low recombination rate due to the indirect nature of the low energy transition. Looking at other compositions like $MAPbBr_3$ and using higher pressures two phase transitions and a reversible amorphization have been shown by PL.[123][124] Similar studies have been performed on most other compositions and an overview about pressure induced effect can be found elsewhere.[125][126]

4. UV-Vis

Complementary to PL where the de-excitation from an excited state to the ground state is probed, UV-Vis spectroscopy investigates the wavelength dependent excitation of charge carriers from the ground state to an excited state. For this typically a broad light spectrum reaching from the near ultra violet to the near infrared region is used to excite charge carriers. Depending on the measurement configuration, light transmission or reflection is measured. Similar to PL, the detected light can be measured in one shot using a detector array or by scanning through the wavelengths with a monochromator. It should be noted that UV-VIS measurements are normally relative in comparison to a reference sample, which can be a substrate without active layer or an empty cuvette. In reference[71] more details about UV-Vis measurements and how to interpret the data can be found. It is possible to use the same optical components within one setup for PL and UV-Vis measurements and record both properties quasi-simultaneously as demonstrated by Buchhorn et al. [73] (Figure 2b).

UV-Vis measurements in other fields are widely used to determine concentrations of additives in solution or to investigate conjugated polymers and their vibronic structure. In organic PV it is possible with *in situ* UV-Vis measurements to investigate how polymer chains orientate (formation of J and H aggregates) in the drying films from which the electronic properties of the finished thin films can be predicted.[127][128] In the field of perovskite solar cells UV-Vis spectroscopy is mostly used to investigate the total absorbance which is the logarithm of the ratio

between transmitted and incident light. Since in practice the incoming light can fluctuate the transmitted light through the sample is divided by the reference measurement. From the absorption on-set in a UV-Vis spectrum, the bandgap as well as Urbach tailing can be derived. In the following a few examples on how *in situ* UV-Vis measurements are used in literature and what information can be gained will be given.

4.1 Monitoring of Synthesis

Since absorbance is extracted from UV-Vis measurements, it can be deployed to track the formation of light absorbing layers and particles. An early example for the usage of UV-Vis to study the synthesis and alloying of $MAPbI_3$ with chloride is given by Unger at al.[26] The absorption of the precursor was studied during one hour of annealing (Figure 8a). Within the first 30 minutes the absorption below 740 nm continuously increases indicating the formation of $MAPb(Cl,I)_3$. After this the absorption is constant hinting that the reaction is complete. Comparing the absorption traces at 570 nm and 740 nm (Figure 8b) illustrates that initially the absorption at lower wavelengths increases, possibly related to the formation of an intermediate phase before the formation of $MAPb(Cl,I)_3$.

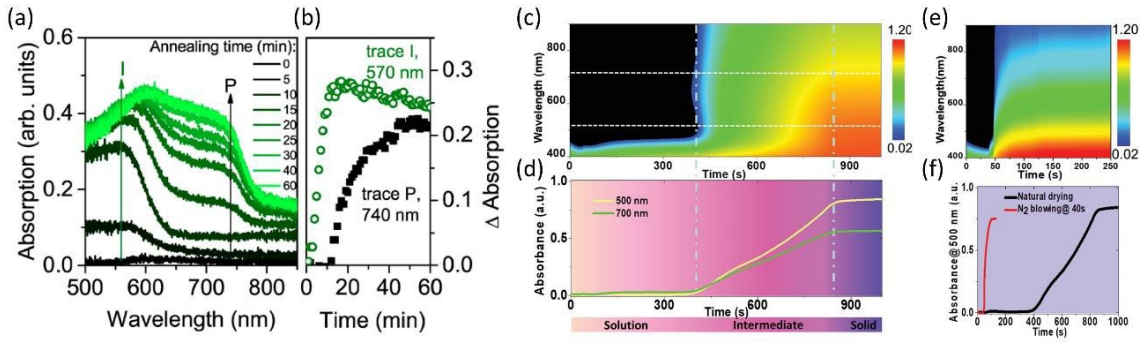

Figure 8: a) Change of absorption with time during annealing of $MAPb(Cl,I)_3$ sample b) Profile of absorption at 570 nm and at 740 nm over time. Reproduced with permission.[26] Copyright 2014, American Chemical Society.
c)Time resolved UV-Vis absorption of a drying perovskite film coated by blade coating d) Absorbance of the same drying process at 500 nm and 700 nm e) first 250 seconds of an air-knife-assisted drying process. f) Absorbance at 500 nm of both drying processes. Reproduced with permission.[27] Copyright 2019, Wiley-VCH.

Several techniques have been successfully implemented to deposit halide perovskite thin films on different length scales each with specific

crystallization dynamics.[8] A good example on how *in situ* UV-Vis can be used to investigate the crystallization during those deposition methods is given by Hu et al.[27] They investigated the drying kinetics of $Cs_{0.05}FA_{0.81}MA_{0.14}PbI_{2.55}Br_{0.45}$ films deposited by meniscus blade coating. Measuring the UV-Vis absorption of a natural drying layer, three distinguished stages are observed (Figure 8c-d).

Within the first 390 s no absorption is observed at 500 nm, indicating a low concentration of solids in the solution and no nucleation occurring. In the second stage the absorption increases due to nucleation and crystal growth induced by the increasing concentration due to solvent evaporation. After roughly 850 s the absorbance stabilizes showing the film formation process is completed. However, this natural drying process leads to inhomogeneous film formation with poor coverage. To improve the drying kinetics a laminar airflow of N_2 is added 40 s after the deposition. Within seconds after the air flow is initiated a strong increase in the absorbance at 500 nm is observed which saturates within another few seconds (Figure 8e). Comparing the absorbance of the two drying processes (Figure 8f) a nearly two order faster growth for the air- knife assisted process is measured. The usage of N_2 thus greatly accelerates solvent drying, gives a better solvent evaporation control and yields homogenous thin films after annealing.

Yamada et al.[129] used UV-Vis to track the crystallization on longer time scales. They investigate $MAPbI_3$ samples which are formed by depositing a PbI_2 layer by spin coating, followed by a dip in MAI solution and annealing on a hotplate. PL shows a clear improvement in the decay time over the course of 75 hours which can be explained by looking at the UV-Vis data. The data exhibits a clearly defined absorption edge at 1.6 eV corresponding to the bandgap of the formed $MAPbI_3$ layer, but also a second absorption on-set at 2.4 eV corresponding to the bandgap of unreacted PbI_2. Over time the high energy absorption edge decreases

indicating consumption of PbI_2 to form perovskite. The same measurements also showed an improvement in the steepness of the absorption edge of the $MAPbI_3$ likely related to a better crystal structure. Looking at the absorption on-sets of the different constituents can thus be used to track crystallization processes.

Besides studying crystallization dynamics, tracking of ion exchange processes is possible with UV-Vis measurements. The cation exchange for the $(FA,MA)PbI_3$ system was shown for nanocrystals by Hills-Kimball et al. [130] and for thin films by Eperon et al.[95] Additionally, the

suppression of anion exchange in between nanocrystals by oleate capping was studied with *in situ* UV-Vis by Ravi et al.[29]

Although not a real *in situ* measurement technique, it should be mentioned that the reflection spectrum from a solution during spin coating or blade coating can be used to determine the film thickness and thus to fine tune the process. Due to thin film interference the reflection profile of those films exhibit plenty of interference peaks, which with knowledge of the refractive index of the film can be used to calculate the film thickness. [131] For perovskites this has been shown to yield good process control for spin coating [21] as well as blade coating.[132]

4.2 Ion Migration and Sample Degradation

As discussed in the PL part, the understanding of degradation behaviors and pathways is crucial to advance perovskite solar cells. Similar to PL, UV-Vis can be used to track ion migration, although only on a larger lateral scale. A recent example for this is given by Scheidt et al.[28] who investigated the ion migration in graded $CsPbI_{3-x}Br_x$ thin films. A graded sample initially shows absorption both around 575 nm from bromide-rich regions and at roughly 650 nm from iodide-rich regions (Figure 9a). With ongoing annealing, the absorption around 650-700 nm diminishes and the absorption edge of the bromide-rich phase at 575 nm shows a red shift. Both features indicate a homogenization of the film. A mono exponential growth is observed when plotting the absorbance at 600 nm over time

(Figure 9b) which can be fitted to extract the rate constant. Repeating this experiment at several temperature ranging from 40 °C to 90 °C gives the temperature dependent rate constant. Plotting them in an Arrhenius plot, an activation energy for the anion exchange of about 75 kJ/mol is determined reflecting the barrier for halide ion mobility in cesium lead perovskites.

Regarding the influence of the surrounding atmosphere on $MAPbI_3$ samples Senocrate et al.[133] published a comprehensive study on the effect of O_2. In the experiment UV-Vis measurements are carried out periodically over the course of 150 hours for three sample storing conditions each including O_2 (Figure 9c). The first sample was stored in the dark and is stable showing hardly any changes in absorbance. However, under light the sample nearly completely decomposed within 40 hours. Looking at the bandgap absorption it can be derived that the decay is constant in the beginning and then enhances drastically after about 30 hours (Figure 9d). This is explained by a decomposition reaction in which water and iodide is formed. The formed water then enhances the degradation leading faster decay in absorption. By supplying iodide the chemical balance of the decomposition reaction can be shifted and thus the degradation slowed down. Experimentally a two times slower degradation is observed when iodide is supplied, affirming the theory. However, looking at the sub-bandgap absorption a broader tail is observed for this condition indicating an amorphization of the perovskite layer.

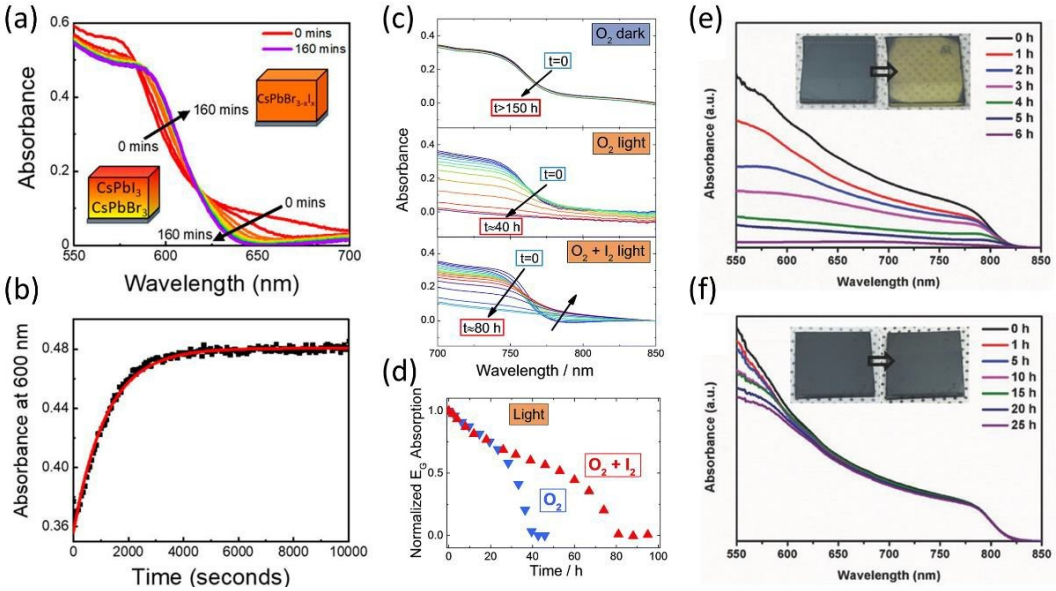

Figure 9: a) Absorbance of a graded $CsPbI_{3-x}Br_x$ sample measured during annealing at 90 °C for 160 minutes. b) Change in absorbance at 600 nm plotted over elapse time of the annealing process. Reproduced with permission.[28] Copyright 2019, AIP Publishing LLC. c) Absorbance of $MAPbI_3$ samples measured by UV-Vis for extended periods of time under different conditions. d) Normalized absorption at the bandgap over time for a $MAPbI_3$ sample under O_2 and light as well as with additional iodide particle pressure. Reproduced with permission.[133] Copyright 2018, Royal Society of Chemistry. Absorbance of a $FAPbI_3$ e) and a $RbFAPbI_3$ f) sample during exposure to 85% RH in the dark. Reproduced with permission.[30] Copyright 2017, Wiley-VCH.

Furthermore, the degradation under ambient and humid conditions is well studied by *in situ* UV-Vis measurements. Early studies showed the poor stability of $MAPbI_3$ samples in humid conditions.[44][46][57][134]–[136] But also in dry condition instabilities were observed and traced back to the illumination conditions.[46][134][137]–[139] Using mixed cation perovskite the stability can be greatly improved.[7][13][30][140]–[143] One example for this is the addition of rubidium to $FAPbI_3$ as shown by Park et al.[30] The absorbance of a pure $MAPbI_3$ degrades in the dark under highly humid conditions within a few hours (Figure 9e). By adding a small amount of rubidium, the tolerance against moisture is greatly increased resulting in no change in absorbance within 24 hours (Figure 9f). Finally, using a mixture of 2D and 3D perovskites leads to enhancements in the stability, without a change in absorbance under ambient conditions for 40 days.[144] [145] Besides making the absorber layer more robust, the usage of passivating transport layers with hydrophilic properties has been tested and promising results have been reported.[146][147]

4.3 Monitoring Phase TransitionsInduced by Temperature and Pressure

Similar to PL, UV-Vis can be used to study phase transitions induced by temperature or pressure. An early study for the temperature dependent phase transition from the tetragonal to the orthorhombic phase in $MAPb(I,Cl)_3$ samples was published by Wehrenfennig et al.[148] During the heating of the sample from 4 K to room temperature a clear shift in the absorption edge around 140 K was observed (Figure 10a). Surprisingly,

this shift occurs at 120 K during cooling of the sample (Figure 10b). If slower heating and cooling rates are used even larger differences can be measured, revealing a large hysteresis. Looking closer at the shape of the UV-Vis data a peak above the absorption edge attributed to resonant formation of excitons is observed, especially at low temperatures. By studying the decay of the peak and the broadening of the absorption onset with increasing temperatures, the exciton binding energy can be determined.[149]

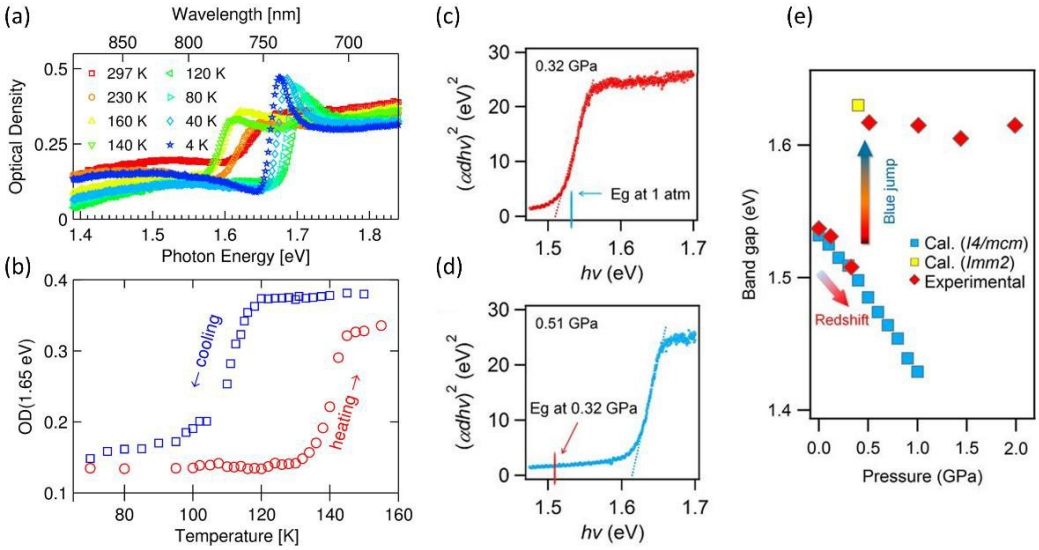

Figure 10: a) Optical density of a $MAPbI_{3-x}Cl_x$ sample measured while heating from 4 K to 297 K. b) Optical density at 1.65 eV during cooling from 160 K to 40 K (blue squares) as well as heating (red circles). Reproduced with permission.[148] Copyright 2014, AIP Publishing LLC. c-d) Direct bandgap Tauc plots of a $MAPbI_3$ sample measured at different pressure conditions. e) Comparison of measured bandgap and theoretical calculation for two different crystal structures. Reproduced with permission.[150] Copyright 2016, National Academy of Sciences.

Also phase transition with pressure are broadly studied with UV-Vis, since using Tauc plots the bandgap can be closely followed. For instance Kong et al.[150] investigated $MAPbI_3$ single crystals and found that with increasing pressure the determined bandgap initially decreases (Figure 10c). Increasing the pressure above 0.5 GPa induces a jump in the bandgap which afterwards is stable (Figure 10d-e). This jump was explained by a phase transition from the tetragonal I4/mcm to the orthorhombic Imm2 phase for $MAPbI_3$ as verified by theoretical calculations.

In another application Li et al.[151] used pressure and relaxation to engineer the relatively high bandgap of the $Cs_2AgBiBr_6$ double perovskite. Also the investigation of nanocrystals is possible and can for instance show a clear splitting of bound excitons with increasing pressure.[152]

5. Conclusions and Outlook

In this review we have described case studies that demonstrate the rich information that can be extracted by using the complementary optical techniques PL and UV-Vis *in situ*. Topics covered are monitoring of synthesis, nucleation and growth, compositional tailoring via ion exchange reactions, as well as degradation, ionic movement, and phase transitions. All the aforementioned phenomena have in common that they translate into bandgap changes which can be correlated to PL emission and UV-Vis absorption. We show that PL and UV-Vis not only provide valuable information when monitoring synthesis but also when investigating temporal evolution of properties (often referred to as “during light soaking” or “under continuous laser irradiation”) including optical and structural properties, and elemental diffusion, under various stimuli such as light, electrical bias, temperature, chemical gradients, and mechanical forces. Importantly, these measurements provide insights about fast processes happening at the seconds and sub-seconds time scales which are not as easily accessible otherwise. In fact, several advances made in the field were catalyzed by *in situ* PL and UV-Vis measurements. For example, *in situ* PL (or “continuous PL”) measurements revealed halide movement in mixed halide perovskites and still is the key technique to investigate transient changes related to mass transport under illumination. PL and UV-Vis nicely show temperature dependent phase transitions including spatially resolved non-uniform phase transitions. Finally, both techniques are very valuable in studying nucleation, growth and material formation where PL provides spectrally resolved information on nucleation

kinetics and UV-Vis complementary information on presence of intermediate phases during material formation.

Since underlying optoelectronic properties govern device performance it is important to correlate their origin and understand their evolution with respect to synthetic variables and/or external parameters such as light, heat, atmosphere. Combining optical probes (PL or UV-Vis) with complementary characterizations recorded simultaneously can provide a powerful holistic

picture of mechanisms that drive processes at different time and length scales. As an example, PL combined with diffraction, scanning electron microscopy or atomic force microscopy can reveal structure-morphology-property relationships. Additionally, and highly relevant for device operation, is information gathered from PL of halide perovskites exposed to electric fields. The latter combination can provide insights into migration and accumulation of mobile ions induced by the presence of electric fields with different processes happening in proximity to the contacts versus away from the contacts. Using calibrated PL measurements (PL quantum yield) in the above outlined experiments can enable quantitative information on the temporal evolution of recombination mechanisms. Finally, as stability is one of the major concerns for hybrid halide perovskite-based technologies, PL and UV-Vis measurements can be powerful to study degradation mechanisms and kinetics under elevated temperature and/or in different atmospheres.

To summarize, we believe that further and possibly more advanced *in situ* optical measurements applied to halide perovskites will significantly advance the field with respect to the understanding of fundamental dynamic processes on both, macroscopic and microscopic levels and therefore, help to enhance performance and stability.

Acknowledgements

This manuscript was prepared with support from the Laboratory Directed Research and Development (LDRD) program of Lawrence Berkeley National Laboratory under U.S. Department of Energy contract number

DE-AC02-05CH11231(C.M.S.-F.). This material is based upon work performed by the Joint Center for Artificial Photosynthesis, a DOE Energy Innovation Hub, supported through the Office of Science of the U.S. Department of Energy under Award Number DE-SC0004993 (F.B.).

Received: ((will be filled in by the editorial staff)) Revised: ((will be filled in by the editorial staff)) Published online: ((will be filled in by the editorial staff))

References

[1] L.M. Herz, *Annu. Rev. Phys. Chem.* **2016**, *67*, 65.
[2] T.M. Brenner, D.A. Egger, L. Kronik, G. Hodes, D. Cahen, *Nat. Rev. Mater.* **2016**, *1*, 15007.
[3] L. Mao, C.C. Stoumpos, M.G. Kanatzidis, *J. Am. Chem. Soc.* **2019**, *141*, 1171.
[4] S. De Wolf, J. Holovsky, S.-J. Moon, P. Löper, B. Niesen, M. Ledinsky, F.-J. Haug, J.-
H. Yum, C. Ballif, *J. Phys. Chem. Lett.* **2014**, *5*, 1035.
[5] S.D. Stranks, R.L.Z. Hoye, D. Di, R.H. Friend, F. Deschler, *Adv. Mater.* **2018**,
1803336, 1803336.
[6] J.H. Noh, S.H. Im, J.H. Heo, T.N. Mandal, S. Il Seok, *Nano Lett.* **2013**, *13*, 1764.
[7] M. Saliba, T. Matsui, J.-Y. Seo, K. Domanski, J.-P. Correa-Baena, M.K. Nazeeruddin,
S.M. Zakeeruddin, W. Tress, A. Abate, A. Hagfeldt, M. Grätzel, *Energy Environ. Sci.*
2016, *9*, 1989.
[8] W.A. Dunlap-Shohl, Y. Zhou, N.P. Padture, D.B. Mitzi, *Chem. Rev.* **2019**, *119*, 3193.
[9] A. Kojima, K. Teshima, Y. Shirai, T. Miyasaka, *J. Am. Chem. Soc.* **2009**, *131*, 6050.
[10] M.M. Lee, J. Teuscher, T. Miyasaka, T.N. Murakami, H.J. Snaith, *Science* **2012**, *338*, 643.
[11] G.E. Eperon, S.D. Stranks, C. Menelaou, M.B. Johnston, L.M. Herz, H.J. Snaith,
Energy Environ. Sci. **2014**, *7*, 982.
[12] T. Duong, Y. Wu, H. Shen, J. Peng, X. Fu, D. Jacobs, E.-C. Wang, T.C. Kho, K.C. Fong, M. Stocks, E. Franklin, A. Blakers, N. Zin, K. McIntosh, W. Li, Y.-B. Cheng,
T.P. White, K. Weber, K. Catchpole, *Adv. Energy Mater.* **2017**, 1700228.
[13] L.K. Ono, E.J. Juarez-Perez, Y. Qi, *ACS Appl. Mater. Interfaces* **2017**, *9*, 30197.
[14] National Renewable Energy Laboratory efficiency chart, https://www.nrel.gov/pv/cell- efficiency.html, last visited 02/13/2020.
[15] A.Y. Alsalloum, B. Turedi, X. Zheng, S. Mitra, A.A. Zhumekenov, K.J. Lee, P. Maity,
I. Gereige, A. AlSaggaf, I.S. Roqan, O.F. Mohammed, O.M. Bakr, *ACS*

Energy Lett. **2020**, 657.
[16] A. Walsh, S.D. Stranks, *ACS Energy Lett.* **2018**, *3*, 1983.
[17] Q. Hu, L. Zhao, J. Wu, K. Gao, D. Luo, Y. Jiang, Z. Zhang, C. Zhu, E. Schaible, A. Hexemer, C. Wang, Y. Liu, W. Zhang, M. Grätzel, F. Liu, T.P. Russell, R. Zhu, Q. Gong, *Nat. Commun.* **2017**, *8*, 15688.
[18] T. Miyadera, Y. Shibata, T. Koganezawa, T.N. Murakami, T. Sugita, N. Tanigaki, M. Chikamatsu, *Nano Lett.* **2015**, *15*, 5630.
[19] D.T. Moore, H. Sai, K.W. Tan, D.-M. Smilgies, W. Zhang, H.J. Snaith, U. Wiesner,
L.A. Estroff, *J. Am. Chem. Soc.* **2015**, *137*, 2350.
[20] W. Zhang, M. Saliba, D.T. Moore, S.K. Pathak, M.T. Hörantner, T. Stergiopoulos, S.D. Stranks, G.E. Eperon, J.A. Alexander-Webber, A. Abate, A. Sadhanala, S. Yao, Y. Chen, R.H. Friend, L.A. Estroff, U. Wiesner, H.J. Snaith, *Nat. Commun.* **2015**, *6*, 6142.
[21] R. Munir, A.D. Sheikh, M. Abdelsamie, H. Hu, L. Yu, K. Zhao, T. Kim, O. El Tall, R. Li, D.-M. Smilgies, A. Amassian, *Adv. Mater.* **2017**, *29*, 1604113.

[22] D.P. Nenon, J.A. Christians, L.M. Wheeler, J.L. Blackburn, E.M. Sanehira, B. Dou,
M.L. Olsen, K. Zhu, J.J. Berry, J.M. Luther, *Energy Environ. Sci.* **2016**, *9*, 2072.
[23] S.J. Park, A.R. Kim, J.T. Hong, J.Y. Park, S. Lee, Y.H. Ahn, *J. Phys. Chem. Lett.* **2017**,
8, 401.
[24] R.L. Milot, G.E. Eperon, H.J. Snaith, M.B. Johnston, L.M. Herz, *Adv. Funct. Mater.*
2015, *25*, 6218.
[25] C. La-o-vorakiat, H. Xia, J. Kadro, T. Salim, D. Zhao, T. Ahmed, Y.M. Lam, J.-X. Zhu, R.A. Marcus, M.-E. Michel-Beyerle, E.E.M. Chia, *J. Phys. Chem. Lett.* **2016**, *7*, 1.
[26] E.L. Unger, A.R. Bowring, C.J. Tassone, V.L. Pool, A. Gold-Parker, R. Cheacharoen,
K.H. Stone, E.T. Hoke, M.F. Toney, M.D. McGehee, *Chem. Mater.* **2014**, *26*, 7158.
[27] H. Hu, Z. Ren, P.W.K. Fong, M. Qin, D. Liu, D. Lei, X. Lu, G. Li, *Adv. Funct. Mater.*
2019, *29*, 1.
[28] R.A. Scheidt, P.V. Kamat, *J. Chem. Phys.* **2019**, *151*, 134703.
[29] V.K. Ravi, R.A. Scheidt, A. Nag, M. Kuno, P.V. Kamat, *ACS Energy Lett.* **2018**, *3*, 1049.
[30] Y.H. Park, I. Jeong, S. Bae, H.J. Son, P. Lee, J. Lee, C.-H. Lee, M.J. Ko, *Adv. Funct. Mater.* **2017**, *27*, 1605988.
[31] J.A. Aguiar, S. Wozny, T.G. Holesinger, T. Aoki, M.K. Patel, M. Yang, J.J. Berry, M. Al-Jassim, W. Zhou, K. Zhu, *Energy Environ. Sci.* **2016**, *9*, 2372.
[32] S. Ruan, M.-A. Surmiak, Y. Ruan, D.P. McMeekin, H. Ebendorff-Heidepriem, Y.-B. Cheng, J. Lu, C.R. McNeill, *J. Mater. Chem. C* **2019**, *7*, 9326.
[33] J.J. van Franeker, K.H. Hendriks, B.J. Bruijnaers, M.W.G.M. Verhoeven, M.M. Wienk,
R.A.J. Janssen, *Adv. Energy Mater.* **2017**, *7*, 1601822.
[34] T. Song, Z. Yuan, M. Mori, F. Motiwala, G. Segev, E. Masquelier, C.V. Stan, J.L. Slack, N. Tamura, C.M. Sutter-Fella, *Adv. Funct. Mater.* **2019**, 1908337.
[35] R. Brenes, C. Eames, V. Bulović, M.S. Islam, S.D. Stranks, *Adv. Mater.* **2018**, *30*, 1.
[36] W.A. Quitsch, D.W. Dequilettes, O. Pfingsten, A. Schmitz, S. Ognjanovic, S. Jariwala,
S. Koch, M. Winterer, D.S. Ginger, G. Bacher, *J. Phys. Chem. Lett.* **2018**, *9*, 2062.
[37] Y. Zhao, H. Tan, H. Yuan, Z. Yang, J.Z. Fan, J. Kim, O. Voznyy, X. Gong, L.N. Quan,
C.S. Tan, J. Hofkens, D. Yu, Q. Zhao, E.H. Sargent, *Nat. Commun.* **2018**, *9*, 1607.
[38] K. Galkowski, A.A. Mitioglu, A. Surrente, Z. Yang, D.K. Maude, P. Kossacki, G.E. Eperon, J.T.W. Wang, H.J. Snaith, P. Plochocka, R.J. Nicholas, *Nanoscale* **2017**, *9*, 3222.

[39] M. Do, I. Kim, M.A. Kolaczkowski, J. Kang, G.A. Kamat, Z. Yuan, N.S. Barchi, L.-W. Wang, Y. Liu, M.J. Jurow, C.M. Sutter-Fella, *Nanoscale* **2019**.
[40] T.-B. Song, Z. Yuan, F. Babbe, D.P. Nenon, E. Aydin, S. De Wolf, C.M. Sutter-Fella,
accepted for publication in ACS Applied Energy Materials**.**
[41] K. Domanski, E.A. Alharbi, A. Hagfeldt, M. Grätzel, W. Tress, *Nat. Energy* **2018**, *3*, 61.
[42] C.C. Boyd, R. Cheacharoen, T. Leijtens, M.D. McGehee, *Chem. Rev.* **2019**, *119*, 3418.
[43] M.I.H. Ansari, A. Qurashi, M.K. Nazeeruddin, *J. Photochem. Photobiol. C Photochem. Rev.* **2018**, *35*, 1.
[44] J. Yang, B.D. Siempelkamp, D. Liu, T.L. Kelly, *ACS Nano* **2015**, *9*, 1955.
[45] H. Gao, C. Bao, F. Li, T. Yu, J. Yang, W. Zhu, X. Zhou, G. Fu, Z. Zou, *ACS Appl. Mater. Interfaces* **2015**, *7*, 9110.
[46] D. Bryant, N. Aristidou, S. Pont, I. Sanchez-Molina, T. Chotchunangatchaval, S. Wheeler, J.R. Durrant, S.A. Haque, *Energy Environ. Sci.* **2016**, *9*, 1655.
[47] S.J. Yoon, S. Draguta, J.S. Manser, O. Sharia, W.F. Schneider, M. Kuno, P.V. Kamat,
ACS Energy Lett. **2016**, *1*, 290.
[48] X. Deng, X. Wen, C.F.J. Lau, T. Young, J. Yun, M.A. Green, S. Huang, A.W.Y. Ho- Baillie, *J. Mater. Chem. C* **2016**, *4*, 9060.

[49] A. Miyata, A. Mitioglu, P. Plochocka, O. Portugall, J.T.-W. Wang, S.D. Stranks, H.J. Snaith, R.J. Nicholas, *Nat. Phys.* **2015**, *11*, 582.
[50] S.D. Stranks, V.M. Burlakov, T. Leijtens, J.M. Ball, A. Goriely, H.J. Snaith, *Phys. Rev. Appl.* **2014**, *2*, 034007.
[51] F. Staub, H. Hempel, J.C. Hebig, J. Mock, U.W. Paetzold, U. Rau, T. Unold, T. Kirchartz, *Phys. Rev. Appl.* **2016**, *6*, 1.
[52] Y. Tian, M. Peter, E. Unger, M. Abdellah, K. Zheng, T. Pullerits, A. Yartsev, V. Sundström, I.G. Scheblykin, *Phys. Chem. Chem. Phys.* **2015**, *17*, 24978.
[53] E.T. Hoke, D.J. Slotcavage, E.R. Dohner, A.R. Bowring, H.I. Karunadasa, M.D. McGehee, *Chem. Sci.* **2014**, *6*, 613.
[54] D.W. DeQuilettes, W. Zhang, V.M. Burlakov, D.J. Graham, T. Leijtens, A. Osherov,
V. Bulović, H.J. Snaith, D.S. Ginger, S.D. Stranks, *Nat. Commun.* **2016**, *7*.
[55] A.J. Knight, A.D. Wright, J.B. Patel, D.P. McMeekin, H.J. Snaith, M.B. Johnston, L.M. Herz, *ACS Energy Lett.* **2019**, *4*, 75.
[56] R. Gottesman, L. Gouda, B.S. Kalanoor, E. Haltzi, S. Tirosh, E. Rosh-Hodesh, Y. Tischler, A. Zaban, C. Quarti, E. Mosconi, F. De Angelis, *J. Phys. Chem. Lett.* **2015**, *6*, 2332.
[57] N. Ahn, K. Kwak, M.S. Jang, H. Yoon, B.Y. Lee, J.-K. Lee, P.V. Pikhitsa, J. Byun, M. Choi, *Nat. Commun.* **2016**, *7*, 13422.
[58] S. Chen, X. Wen, R. Sheng, S. Huang, X. Deng, M.A. Green, A. Ho-Baillie, *ACS Appl. Mater. Interfaces* **2016**, *8*, 5351.
[59] X. Deng, X. Wen, J. Zheng, T. Young, C.F.J. Lau, J. Kim, M. Green, S. Huang, A. Ho- Baillie, *Nano Energy* **2018**, *46*, 356.
[60] W. Mao, C.R. Hall, A.S.R. Chesman, C. Forsyth, Y.B. Cheng, N.W. Duffy, T.A. Smith, U. Bach, *Angew. Chem. - Int. Ed.* **2019**, *58*, 2893.
[61] T.P. Gujar, T. Unger, A. Schönleber, M. Fried, F. Panzer, S. van Smaalen, A. Köhler,
M. Thelakkat, *Phys. Chem. Chem. Phys.* **2018**, *20*, 605.
[62] S. Chen, X. Wen, S. Huang, F. Huang, Y.-B. Cheng, M. Green, A. Ho-Baillie, *Sol. RRL*
2017, *1*, 1600001.
[63] X. Yang, X. Yan, W. Wang, X. Zhu, H. Li, W. Ma, C. Sheng, *Org. Electron.* **2016**, *34*, 79.
[64] H. Yuan, E. Debroye, K. Janssen, H. Naiki, C. Steuwe, G. Lu, M. Moris, E. Orgiu, H. Uji-i, F. De Schryver, P. Samorì, J. Hofkens, M. Roeffaers, *J. Phys. Chem. Lett.* **2016**, *7*, 561.
[65] J.F. Galisteo-López, M. Anaya, M.E. Calvo, H. Míguez, *J. Phys. Chem. Lett.* **2015**, *6*, 2200.
[66] C.G. Bischak, C.L. Hetherington, H. Wu, S. Aloni, D.F. Ogletree, D.T. Limmer, N.S. Ginsberg, *Nano Lett.* **2017**, *17*, 1028.
[67] M.A. Green, Y. Jiang, A.M. Soufiani, A. Ho-Baillie, *J. Phys. Chem. Lett.* **2015**, *6*, 4774.
[68] P.Y. Yu, M. Cardona, *Fundamentals of Semiconductors*, Springer Berlin Heidelberg, Berlin, Heidelberg **2010**.
[69] C.F. Klingshirn, *Semiconductor Optics*, Springer Berlin Heidelberg, Berlin, Heidelberg

2012.
[70] T. Unold, L. Gütay, in *Adv. Charact. Tech. Thin Film Sol. Cells* (Eds: D. Abou-Ras, T. Kirchartz, U. Rau), Wiley-VCH Verlag GmbH & Co. KGaA, Weinheim, Germany **2011**, 151.
[71] A. McClelland, M. Mankin, *Optical Measurements for Scientists and Engineers: A Practical Guide*, Cambridge University Press**2018**.
[72] Y.-M. Xie, B. Yu, C. Ma, X. Xu, Y. Cheng, S. Yuan, Z.-K. Wang, H.T. Chandran, C.-
S. Lee, L.-S. Liao, S.-W. Tsang, *J. Mater. Chem. A* **2018**, *6*, 9081.

[73] M. Buchhorn, S. Wedler, F. Panzer, *J. Phys. Chem. A* **2018**, *122*, 9115.
[74] T.H. Gfroerer, in *Encycl. Anal. Chem.*, John Wiley & Sons, Ltd, Chichester, UK **2006**, 9209.
[75] , Ed: D.R. Vij, *Luminescence of Solids*, Springer US, Boston, MA **1998**.
[76] C.M. Sutter-Fella, Q.P. Ngo, N. Cefarin, K.L. Gardner, N. Tamura, C. V. Stan, W.S. Drisdell, A. Javey, F.M. Toma, I.D. Sharp, *Nano Lett.* **2018**, *18*, 3473.
[77] J.M. Richter, M. Abdi-Jalebi, A. Sadhanala, M. Tabachnyk, J.P.H. Rivett, L.M. Pazos- Outón, K.C. Gödel, M. Price, F. Deschler, R.H. Friend, *Nat. Commun.* **2016**, *7*, 13941.
[78] I.L. Braly, D.W. Dequilettes, L.M. Pazos-Outón, S. Burke, M.E. Ziffer, D.S. Ginger,
H.W. Hillhouse, *Nat. Photonics* **2018**, *12*, 355.
[79] P. Caprioglio, M. Stolterfoht, C.M. Wolff, T. Unold, B. Rech, S. Albrecht, D. Neher,
Adv. Energy Mater. **2019**, *1901631*, 1901631.
[80] P. Wurfel, *J. Phys. C Solid State Phys.* **1982**, *15*, 3967.
[81] J.K. Larsen, S.-Y. Li, J.J.S. Scragg, Y. Ren, C. Hägglund, M.D. Heinemann, S. Kretzschmar, T. Unold, C. Platzer-Björkman, *J. Appl. Phys.* **2015**, *118*, 035307.
[82] C.M. Sutter-Fella, Y. Li, M. Amani, J.W. Ager, F.M. Toma, E. Yablonovitch, I.D. Sharp, A. Javey, *Nano Lett.* **2016**, *16*, 800.
[83] A. Merdasa, M. Bag, Y. Tian, E. Källman, A. Dobrovolsky, I.G. Scheblykin, *J. Phys. Chem. C* **2016**, *120*, 10711.
[84] A. Merdasa, Y. Tian, R. Camacho, A. Dobrovolsky, E. Debroye, E.L. Unger, J. Hofkens, V. Sundström, I.G. Scheblykin, *ACS Nano* **2017**, *11*, 5391.
[85] I. Lignos, V. Morad, Y. Shynkarenko, C. Bernasconi, R.M. Maceiczyk, L. Protesescu,
F. Bertolotti, S. Kumar, S.T. Ochsenbein, N. Masciocchi, A. Guagliardi, C.J. Shih, M.I. Bodnarchuk, A.J. Demello, M. V. Kovalenko, *ACS Nano* **2018**, *12*, 5504.
[86] L. Huang, Z. Hu, J. Xu, K. Zhang, J. Zhang, Y. Zhu, *Sol. Energy Mater. Sol. Cells*
2015, *141*, 377.
[87] Z. Xiao, Q. Dong, C. Bi, Y. Shao, Y. Yuan, J. Huang, *Adv. Mater.* **2014**, *26*, 6503.
[88] L. Wagner, L.E. Mundt, G. Mathiazhagan, M. Mundus, M.C. Schubert, S. Mastroianni,
U. Würfel, A. Hinsch, S.W. Glunz, *Sci. Rep.* **2017**, *7*, 1.
[89] L. Protesescu, S. Yakunin, M.I. Bodnarchuk, F. Krieg, R. Caputo, C.H. Hendon, R.X. Yang, A. Walsh, M.V. Kovalenko, *Nano Lett.* **2015**, *15*, 3692.
[90] Q.A. Akkerman, S.G. Motti, A.R. Srimath Kandada, E. Mosconi, V. D'Innocenzo, G. Bertoni, S. Marras, B.A. Kamino, L. Miranda, F. De Angelis, A. Petrozza, M. Prato, L. Manna, *J. Am. Chem. Soc.* **2016**, *138*, 1010.
[91] I. Lignos, S. Stavrakis, G. Nedelcu, L. Protesescu, A.J. Demello, M. V. Kovalenko,

Nano Lett. **2016**, *16*, 1869.
[92] L. De Trizio, M. Prato, A. Genovese, A. Casu, M. Povia, R. Simonutti, M.J.P. Alcocer, C. D'Andrea, F. Tassone, L. Manna, *Chem. Mater.* **2012**, *24*, 2400.
[93] N. Pellet, J. Teuscher, J. Maier, M. Grätzel, *Chem. Mater.* **2015**, *27*, 2181.
[94] G. Nedelcu, L. Protesescu, S. Yakunin, M.I. Bodnarchuk, M.J. Grotevent, M. V. Kovalenko, *Nano Lett.* **2015**, *15*, 5635.
[95] G.E. Eperon, C.E. Beck, H.J. Snaith, *Mater. Horiz.* **2016**, *3*, 63.
[96] T.J. Jacobsson, J.-P. Correa-Baena, M. Pazoki, M. Saliba, K. Schenk, M. Grätzel, A. Hagfeldt, *Energy Environ. Sci.* **2016**, *9*, 1706.
[97] D.J. Slotcavage, H.I. Karunadasa, M.D. McGehee, *ACS Energy Lett.* **2016**, *1*, 1199.
[98] H.F. Zarick, N. Soetan, W.R. Erwin, R. Bardhan, *J. Mater. Chem. A* **2018**, *6*, 5507.
[99] A.J. Barker, A. Sadhanala, F. Deschler, M. Gandini, S.P. Senanayak, P.M. Pearce, E. Mosconi, A.J. Pearson, Y. Wu, A.R. Srimath Kandada, T. Leijtens, F. De Angelis, S.E. Dutton, A. Petrozza, R.H. Friend, *ACS Energy Lett.* **2017**, *2*, 1416.
[100] Y. Zhou, Y.-H. Jia, H.-H. Fang, M.A. Loi, F.-Y. Xie, L. Gong, M.-C. Qin, X.-H. Lu, C.-P. Wong, N. Zhao, *Adv. Funct. Mater.* **n.d.**, *0*, 1803130.

[101] R. Brenes, D. Guo, A. Osherov, N.K. Noel, C. Eames, E.M. Hutter, S.K. Pathak, F. Niroui, R.H. Friend, M.S. Islam, H.J. Snaith, V. Bulović, T.J. Savenije, S.D. Stranks, *Joule* **2017**, *1*, 155.
[102] J.M. Howard, E.M. Tennyson, S. Barik, R. Szostak, E. Waks, M.F. Toney, A.F. Nogueira, B.R.A. Neves, M.S. Leite, *J. Phys. Chem. Lett.* **2018**, *9*, 3463.
[103] J. Tian, Q. Xue, X. Tang, Y. Chen, N. Li, Z. Hu, T. Shi, X. Wang, F. Huang, C.J. Brabec, H.-L. Yip, Y. Cao, *Adv. Mater.* **2019**, *31*, 1901152.
[104] W. Fan, Y. Shi, T. Shi, S. Chu, W. Chen, K.O. Ighodalo, J. Zhao, X. Li, Z. Xiao, *ACS Energy Lett.* **2019**, *4*, 2052.
[105] H.-H. Fang, F. Wang, S. Adjokatse, N. Zhao, M.A. Loi, *Adv. Funct. Mater.* **2016**, *26*, 4653.
[106] Z. Song, N. Shrestha, S.C. Watthage, G.K. Liyanage, Z.S. Almutawah, R.H. Ahangharnejhad, A.B. Phillips, R.J. Ellingson, M.J. Heben, *J. Phys. Chem. Lett.* **2018**, *9*, 6312.
[107] X. Tang, M. Van Den Berg, E. Gu, A. Horneber, G.J. Matt, A. Osvet, A.J. Meixner, D. Zhang, C.J. Brabec, *Nano Lett.* **2018**, *18*, 2172.
[108] Y. Zhong, C.A.M. Luna, R. Hildner, C. Li, S. Huettner, *APL Mater.* **2019**, *7*, 041114.
[109] M.H. Futscher, J.M. Lee, L. McGovern, L.A. Muscarella, T. Wang, M.I. Haider, A. Fakharuddin, L. Schmidt-Mende, B. Ehrler, *Mater. Horiz.* **2019**, *6*, 1497.
[110] D.W. de Quilettes, S.M. Vorpahl, S.D. Stranks, H. Nagaoka, G.E. Eperon, M.E. Ziffer,
H.J. Snaith, D.S. Ginger, *Science* **2015**, *348*, 683.
[111] S. Draguta, J.A. Christians, Y.V. Morozov, A. Mucunzi, J.S. Manser, P.V. Kamat, J.M. Luther, M. Kuno, *Energy Environ. Sci.* **2018**, *11*, 960.
[112] S. Draguta, S. Thakur, Y.V. Morozov, Y. Wang, J.S. Manser, P.V. Kamat, M. Kuno, *J. Phys. Chem. Lett.* **2016**, *7*, 715.
[113] G. El-Hajje, C. Momblona, L. Gil-Escrig, J. Ávila, T. Guillemot, J.-F. Guillemoles, M. Sessolo, H.J. Bolink, L. Lombez, *Energy Environ. Sci.* **2016**, *9*, 2286.
[114] S.Y. Leblebici, L. Leppert, Y. Li, S.E. Reyes-Lillo, S. Wickenburg, E. Wong, J. Lee,
M. Melli, D. Ziegler, D.K. Angell, D.F. Ogletree, P.D. Ashby, F.M. Toma, J.B. Neaton,
I.D. Sharp, A. Weber-Bargioni, *Nat. Energy* **2016**, *1*, 16093.
[115] A.D. Wright, C. Verdi, R.L. Milot, G.E. Eperon, M.A. Pérez-Osorio, H.J. Snaith, F. Giustino, M.B. Johnston, L.M. Herz, *Nat. Commun.* **2016**, *7*.
[116] K. Wu, A. Bera, C. Ma, Y. Du, Y. Yang, L. Li, T. Wu, *Phys Chem Chem Phys* **2014**,
16, 22476.
[117] X. Wu, M.T. Trinh, D. Niesner, H. Zhu, Z. Norman, J.S. Owen, O. Yaffe, B.J. Kudisch, X.-Y. Zhu, *J. Am. Chem. Soc.* **2015**, *137*, 2089.
[118] H.H. Fang, L. Protesescu, D.M. Balazs, S. Adjokatse, M. V. Kovalenko, M.A. Loi,

Small **2017**, *13*, 1.
[119] O. Pfingsten, J. Klein, L. Protesescu, M.I. Bodnarchuk, M. V. Kovalenko, G. Bacher, *Nano Lett.* **2018**, *18*, 4440.
[120] M. Fu, P. Tamarat, J.B. Trebbia, M.I. Bodnarchuk, M. V. Kovalenko, J. Even, B. Lounis, *Nat. Commun.* **2018**, *9*, 1.
[121] J.A. Steele, P. Puech, B. Monserrat, B. Wu, R.X. Yang, T. Kirchartz, H. Yuan, G. Fleury, D. Giovanni, E. Fron, M. Keshavarz, E. Debroye, G. Zhou, T.C. Sum, A. Walsh, J. Hofkens, M.B.J. Roeffaers, *ACS Energy Lett.* **2019**, 2205.
[122] T. Wang, B. Daiber, J.M. Frost, S.A. Mann, E.C. Garnett, A. Walsh, B. Ehrler, *Energy Environ. Sci.* **2017**, *10*, 509.
[123] Y. Wang, X. Lü, W. Yang, T. Wen, L. Yang, X. Ren, L. Wang, Z. Lin, Y. Zhao, *J. Am. Chem. Soc.* **2015**, *137*, 11144.
[124] A. Jaffe, Y. Lin, C.M. Beavers, J. Voss, W.L. Mao, H.I. Karunadasa, *ACS Cent. Sci.* **2016**, *2*, 201.

[125] P. Postorino, L. Malavasi, *J. Phys. Chem. Lett.* **2017**, *8*, 2613.
[126] A. Jaffe, Y. Lin, H.I. Karunadasa, *ACS Energy Lett.* **2017**, *2*, 1549.
[127] M. Abdelsamie, K. Zhao, M.R. Niazi, K.W. Chou, A. Amassian, *J. Mater. Chem. C* **2014**, *2*, 3373.
[128] T. Li, J. Benduhn, Z. Qiao, Y. Liu, Y. Li, R. Shivhare, F. Jaiser, P. Wang, J. Ma, O. Zeika, D. Neher, S.C.B. Mannsfeld, Z. Ma, K. Vandewal, K. Leo, *J. Phys. Chem. Lett.* **2019**, *10*, 2684.
[129] Y. Yamada, M. Endo, A. Wakamiya, Y. Kanemitsu, *J. Phys. Chem. Lett.* **2015**, *6*, 482.
[130] K. Hills-Kimball, Y. Nagaoka, C. Cao, E. Chaykovsky, O. Chen, *J. Mater. Chem. C* **2017**, *5*, 5680.
[131] N.S. Güldal, T. Kassar, M. Berlinghof, T. Unruh, C.J. Brabec, *J. Mater. Res.* **2017**, *32*, 1855.
[132] Y. Zhong, R. Munir, J. Li, M.-C. Tang, M.R. Niazi, D.-M. Smilgies, K. Zhao, A. Amassian, *ACS Energy Lett.* **2018**, *3*, 1078.
[133] A. Senocrate, T. Acartürk, G.Y. Kim, R. Merkle, U. Starke, M. Grätzel, J. Maier, *J. Mater. Chem. A* **2018**, *6*, 10847.
[134] G. Murugadoss, S. Tanaka, G. Mizuta, S. Kanaya, H. Nishino, T. Umeyama, H. Imahori, S. Ito, *Jpn. J. Appl. Phys.* **2015**, *54*, 08KF08.
[135] N. Aristidou, C. Eames, I. Sanchez-Molina, X. Bu, J. Kosco, M.S. Islam, S.A. Haque, *Nat. Commun.* **2017**, *8*, 15218.
[136] B. Conings, J. Drijkoningen, N. Gauquelin, A. Babayigit, J. D'Haen, L. D'Olieslaeger, A. Ethirajan, J. Verbeeck, J. Manca, E. Mosconi, F.D. Angelis, H.-G. Boyen, *Adv. Energy Mater.* **2015**, *5*, 1500477.
[137] G. Abdelmageed, L. Jewell, K. Hellier, L. Seymour, B. Luo, F. Bridges, J.Z. Zhang, S. Carter, *Appl. Phys. Lett.* **2016**, *109*, 233905.
[138] S.-W. Lee, S. Kim, S. Bae, K. Cho, T. Chung, L.E. Mundt, S. Lee, S. Park, H. Park, M.C. Schubert, S.W. Glunz, Y. Ko, Y. Jun, Y. Kang, H.-S. Lee, D. Kim, *Sci. Rep.* **2016**, *6*, 38150.
[139] R.J. Stoddard, F.T. Eickemeyer, J.K. Katahara, H.W. Hillhouse, *J. Phys. Chem. Lett.* **2017**, *8*, 3289.
[140] Z. Zhao, F. Gu, H. Rao, S. Ye, Z. Liu, Z. Bian, C. Huang, *Adv. Energy Mater.* **2019**, *9*, 1802671.
[141] Z. Li, M. Yang, J.-S. Park, S.-H. Wei, J.J. Berry, K. Zhu, *Chem. Mater.* **2016**, *28*, 284.
[142] J.-W. Lee, D.-H. Kim, H.-S. Kim, S.-W. Seo, S.M. Cho, N.-G. Park, *Adv. Energy Mater.* **2015**, *5*, 1501310.
[143] Z. Wang, Z. Shi, T. Li, Y. Chen, W. Huang, *Angew. Chem. Int. Ed.* **2017**, *56*, 1190.
[144] C. Ma, C. Leng, Y. Ji, X. Wei, K. Sun, L. Tang, J. Yang, W. Luo, C. Li, Y. Deng, S. Feng, J. Shen, S. Lu, C. Du, H. Shi, *Nanoscale*

2016, *8*, 18309.
[145] L.N. Quan, M. Yuan, R. Comin, O. Voznyy, E.M. Beauregard, S. Hoogland, A. Buin,
A.R. Kirmani, K. Zhao, A. Amassian, D.H. Kim, E.H. Sargent, *J. Am. Chem. Soc.*
2016, *138*, 2649.
[146] M. Kim, S.G. Motti, R. Sorrentino, A. Petrozza, *Energy Environ. Sci.* **2018**, *11*, 2609.
[147] S. Kundu, T.L. Kelly, *Can. J. Chem.* **2019**, *97*, 435.
[148] C. Wehrenfennig, M. Liu, H.J. Snaith, M.B. Johnston, L.M. Herz, *APL Mater.* **2014**, *2*, 081513.
[149] V. D'Innocenzo, G. Grancini, M.J.P. Alcocer, A.R.S. Kandada, S.D. Stranks, M.M. Lee, G. Lanzani, H.J. Snaith, A. Petrozza, *Nat. Commun.* **2014**, *5*, 3586.
[150] L. Kong, G. Liu, J. Gong, Q. Hu, R.D. Schaller, P. Dera, D. Zhang, Z. Liu, W. Yang,
K. Zhu, Y. Tang, C. Wang, S.-H. Wei, T. Xu, H. Mao, *Proc. Natl. Acad. Sci.* **2016**,
113, 8910.

[151] Q. Li, Y. Wang, W. Pan, W. Yang, B. Zou, J. Tang, Z. Quan, *Angew. Chem. Int. Ed.* **2017**, *56*, 15969.
[152] Z. Ma, Z. Liu, S. Lu, L. Wang, X. Feng, D. Yang, K. Wang, G. Xiao, L. Zhang, S.A.T. Redfern, B. Zou, *Nat. Commun.* **2018**, *9*, 4506.

Table of content entry

This review summarizes the advances in the field of halide perovskites making use of optical *in situ* photoluminescence and UV-Vis measurements to investigate dynamic processes including synthesis, ionic movement, degradation, and phase changes.

Keyword: In situ optical monitoring

Finn Babbe, Carolin M. Sutter-Fella*

Title: Optical Absorption-Based *In Situ* Characterization of Halide Perovskites

ToC figure